Technische Universität München

Walther-Meissner-Institut

Bayerische Akademie der Wissenschaften

Fortgeschrittenenpraktikum: The Josephson Parametric Amplifier

Philipp Krüger, Kirill G. Fedorov

Garching – September 10, 2021

In superconducting quantum circuits, such as quantum bits, information is processed and transferred in the form of microwave quantum signals. Moreover, at the end of quantum information protocols, these signals have to be recorded by room temperature electronic devices. Since microwave quantum signals typically consist of very few photons, they must be amplified in order to achieve reasonable signal-to-noise ratios. Therefore, low-noise amplification of quantum signals is crucial. Modern low-noise microwave amplifiers are built upon superconducting Josephson parametric devices, such as a flux-driven Josephson Parametric Amplifier (JPA), which allows to reach the standard quantum limit of amplification and even go beyond it. The current JPA is formed by a superconducting quantum interference device (SQUID) combined with a superconducting coplanar waveguide resonator. The combined system acts as a tunable nonlinear microwave resonator, whose frequency can be varied in-situ via an external magnetic field. A mechanical analogue would be a pendulum of variable length, allowing one to tune its eigenfrequency. Tunability of the nonlinear microwave resonator can be exploited to parametrically pump the JPA via application of a strong microwave signal at twice the resonant frequency. This, in turn, can result in a strong parametric amplification of weak quantum signals incident at the JPA. The same parametric amplification mechanism can be exploited further for generation of genuine quantum signals in the form of squeezed vacuum states.

The students' mission in this practical training is to experimentally study the parametric quantum-limited amplification phenomenon with the flux-driven superconducting JPA. This goal can be split in several parts: (i) analyze the magnetic field dependence of the JPA's resonance frequency via microwave transmission measurements with a Vector Network Analyzer (VNA) and determine the JPA frequency modulation period in terms of the magnetic coil current, (ii) find a suitable working point for parametric amplification and record the corresponding resonance response, (iii) apply a microwave pump signal at an appropriate frequency in order to obtain and measure a substantial parametric amplification gain.

Contents

1 Theory **2**

1.1 Superconductivity and Josephson junctions . . . 2
1.2 Dc-SQUID . . . 6
1.3 Coplanar waveguide resonators . . . 8
1.4 Resonance frequency of the JPA . . . 11
1.5 Parametric amplification with flux-driven JPAs . . . 13
1.6 Additional topic: squeezing with flux-driven JPAs . . . 18

2 Experimental Setup **22**

2.1 JPA sample & microwave packaging . . . 23
2.2 Cryogenic signal routing . . . 24
2.3 Room temperature filters . . . 25
2.4 Electronic measurement equipment . . . 26

3 Measurement **29**

3.1 Safety introduction . . . 29
3.2 Checking the Helium Level . . . 30
3.3 Mounting the dipstick onto the dewar . . . 31
3.4 Cooling down the sample rod . . . 31
3.5 Cryogenic measurements . . . 31
3.6 Warm-up procedure . . . 33

4 Writing the report **35**

4.1 Preparation . . . 35
4.2 Evaluation . . . 35

1 Theory

1.1 Superconductivity and Josephson junctions

One of the most important properties of a superconductor is the Meißner-Ochsenfeld effect, i.e., the expulsion of magnetic flux from the bulk of the superconductor (perfect diamagnetism) below a certain transition temperature. An important consequence of this effect is perfect conductivity which makes superconducting materials a good choice to minimize dissipative losses. All these intriguing effects can be explained by macroscopic quantum nature of the superconducting state, when, under certain conditions, normal electrons may form a quantum condensate of the so-called Cooper pairs (or, superelectrons) with a unified wave function. A direct consequence of the quantum-mechanical coherence of this wave function is magnetic fluxoid quantization in closed superconducting contours. From fundamental point of view, the latter is similar to Bohr-Sommerfeld quantization of normal electron wave function in atoms. Another intriguing phenomenon, which arises from the quantum nature of superelectrons, is the Josephson effect. It has been theoretically predicted by B. Josephson [1]. The Josephson effect can be observed if two superconductors are weakly coupled to each other. This effect can also be understood by considering superconductivity as the quantum-mechanical phenomenon which manifests on macroscopic scales. The Josephson effect originates from the overlap of the wave functions of each superconductor $\Psi_i(\mathbf{r},t) = \sqrt{n_i^*(\mathbf{r},t)}\mathrm{e}^{i\theta_i(\mathbf{r},t)}$, where $i = 1$, 2 denotes superconductor 1 or 2 [2]. Here, $\sqrt{n_i^*(\mathbf{r},t)}$ is the density of superconducting Cooper pairs, and $\theta_i(\mathbf{r},t)$ is the global phase of the wave function for each superconductor. An overlap of the wave functions can be achieved by placing a thin layer of non-superconducting material, such as an insulator, between the two superconductors, as shown in Fig. 1.1 (a). Such a structure is referred to as a Josephson junction. Due to the weak coupling, there can be a finite phase difference across the Josephson junction which will be important to describe the Josephson effect. The gauge invariant phase difference across the Josephson junction is given by [3]

$$\varphi(\mathbf{r},t) = \theta_2(\mathbf{r},t) - \theta_1(\mathbf{r},t) - \frac{2\pi}{\Phi_0}\int_1^2 \mathbf{A}(\mathbf{r},t)\cdot d\mathbf{l}\,, \tag{1.1}$$

where $\Phi_0 = \frac{h}{2e}$ is the magnetic flux quantum and $\mathbf{A}(\mathbf{r},t)$ is a magnetic vector potential. The integration path is along a line from superconductor 1 to superconductor 2. The Josephson effect is commonly described by two equations, the first one being the current-phase relation [4]

$$j_\mathrm{s}(\varphi,\mathbf{r}) = j_\mathrm{c}(\mathbf{r})\sin(\varphi)\,, \tag{1.2}$$

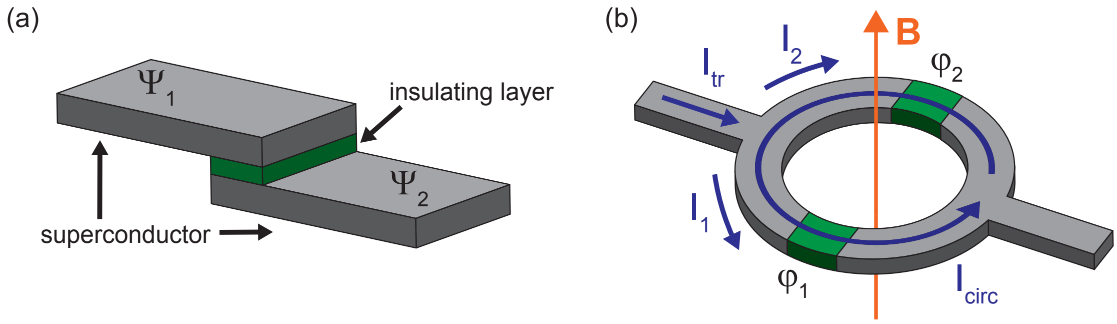

Figure 1.1: (a) Schematic of a Josephson junction with superconductors in gray and an insulating layer in green. (b) Schematic of dc-SQUID with one Josephson junction in each arm of the superconducting loop. Each Josephson junction is associated with a phase difference φ_i.

where $j_{\mathrm{s}}(\varphi, \mathbf{r})$ is the supercurrent density through the Josephson junction and $j_{\mathrm{c}}(\mathbf{r})$ is the critical Josephson current density. For simplicity, we consider spatially homogeneous 0D-systems (with dimensions smaller than the characteristic screening length) and arrive at the first Josephson equation for the total current

$$I_{\mathrm{s}}(\varphi) = I_{\mathrm{c}} \sin(\varphi)\,, \tag{1.3}$$

where I_{s} is the total supercurrent through the Josephson junction and I_{c} is the critical Josephson current of the whole junction.

The second Josephson equation, also called the voltage- or energy-phase relation, describes the time evolution of the phase difference in the presence of a finite energy difference $2eV = \hbar\omega = \hbar\partial\varphi/\partial t$ between the coupled superconductors. That is, it connects the voltage V across a Josephson junction to the time-derivative of the phase difference [4]

$$\frac{\partial\varphi}{\partial t} = \frac{2\pi}{\Phi_0} V(t)\,. \tag{1.4}$$

Consequently, a constant voltage across a Josephson junction leads to a linear evolution of φ in time which, in turn, causes a sinusoidal oscillation of the supercurrent I_{s}.

In this context, it is useful to define the nonlinear inductance $L_{\mathrm{s}} = V(dI_{\mathrm{s}}/dt)^{-1}$ of a Josephson junction [4]

$$L_{\mathrm{s}}(\varphi) = \frac{\Phi_0}{2\pi I_{\mathrm{c}} \cos\varphi} = L_{\mathrm{c}} \frac{1}{\cos\varphi}\,, \tag{1.5}$$

where $L_{\mathrm{c}} = \Phi_0/(2\pi I_{\mathrm{c}})$ corresponds to the minimal Josephson junction inductance. L_{s} can be derived by using the Josephson equations and definition of the inductance $V = L\frac{\mathrm{d}I_{\mathrm{s}}}{\mathrm{d}t}$. The nonlinear properties of a Josephson junction make it a central building block for superconducting circuits where it is often utilized as a nonlinear, lossless inductance.

The dynamics of a Josephson junction can also be described using related energies and potentials. The Josephson coupling energy E_{J} originates from the finite overlap of the wave functions and is defined as $E = \int_0^t V I_s dt = \int_0^\varphi V I_s (dt/d\varphi) d\varphi$ [4]. By substituting the Josephson equations into this integral, one obtains

$$E_{\mathrm{J}}(\varphi) = \frac{\Phi_0 I_{\mathrm{c}}}{2\pi}(1 - \cos\varphi) = E_{\mathrm{J0}}(1 - \cos\varphi)\,, \tag{1.6}$$

where $E_{\mathrm{J0}} = \Phi_0 I_{\mathrm{c}}/2\pi$.

If one drives a Josephson junction with an external current I, acting as a generalized force, the potential energy is given by the tilted washboard potential [5, 4]

$$E_{\mathrm{pot}}(\varphi) = E_{\mathrm{J}}(\varphi) - I\left(\frac{\Phi_0}{2\pi}\varphi\right) = E_{\mathrm{J0}}\left(1 - \cos\varphi - \frac{I}{I_{\mathrm{c}}}\varphi\right)\,. \tag{1.7}$$

To gain an intuitive understanding of the dynamics under the external current I, one can imagine the phase difference φ as a classical particle moving inside this potential. Here, it is important to remember that this classical description of the Josephson junction is valid only in the limit of a large effective mass. The effective mass of the Josephson junction is proportional to its total capacitance C. More specifically, the crossover between the classical and quantum descriptions of the Josephson junction can be described a number of quantized energy levels N in a single isolated period of the corresponding washboard potential. Then, the classical limit can be defined as $N \gg 1$. By approximating the washboard potential with a parabolic function (harmonic approximation), one can show that [4]

$$N \simeq \sqrt{\frac{E_{\mathrm{J}}}{8E_{\mathrm{C}}}} \propto C. \tag{1.8}$$

This equation illustrates the fact that by reducing the junction size, and thereby, its capacitance C, one can eventually enter the quantum regime for the Josephson junction. On contrary, if one wishes to apply the classical description, it is necessary to keep the Josephson junction dimensions relatively large (typically, on the order of few microns, or larger). One can also shunt the junction with a large external capacitance C_{e} in order to increase its total effective capacitance, and respectively, reach the classical regime of $N \gg 1$.

In the classical limit, the zero-voltage state and voltage state of a Josephson junction are related to the phase particle resting and moving in the potential, respectively. The first state can be obtained for $|I| < I_{\mathrm{c}}$, where the particle rests in a local minimum of the potential in the absence of noise sources. The second state corresponds to the phase particle rolling down the potential for $|I| > I_{\mathrm{c}}$, where no local minima exist anymore.

If we consider a Josephson junction with a finite capacitance C and normal resistance R, we can describe the Josephson junction dynamics with the Resistively and Capacitively Shunted Junction (RCSJ) model. This model is only an approximation since it does not consider the superconducting energy gap. The equation of motion within the RCSJ model reads [5, 6]

$$\frac{\ddot{\varphi}}{\omega_{\mathrm{p}}^2} + \frac{\dot{\varphi}}{\omega_{\mathrm{c}}} = j - \sin\varphi = -\frac{1}{E_{\mathrm{J0}}}\frac{\partial E_{\mathrm{pot}}(\varphi)}{\partial\varphi}\,, \tag{1.9}$$

where $\omega_\mathrm{p} = \sqrt{2\pi I_\mathrm{c}/\Phi_0 C}$ is the plasma frequency, $\omega_\mathrm{c} = 2\pi I_\mathrm{c} R/\Phi_0$ a characteristic frequency and $j = I/I_\mathrm{c}$ the normalized supercurrent through the Josephson junction. In principle, Eq. 1.9 can be interpreted as a damped nonlinear LC oscillator. Therefore, the aforementioned plasma frequency ω_p can be viewed as an eigenfrequency of small amplitude phase oscillations in the Josephson junction, while the characteristic frequency ω_c sets the timescale for energy dissipation due to the presence of finite normal resistance.

Alternatively, the dynamics of a Josephson junction can be described with the corresponding Lagrangian. This approach will be useful when investigating more complex scenarios such as the response of JPAs to an applied magnetic flux. If we neglect the resistive term, we obtain the Lagrangian of a single Josephson junction,

$$\mathcal{L} = K(\dot{\varphi}) - E_\mathrm{pot}(\varphi) = \frac{\hbar^2 \dot{\varphi}^2}{4E_\mathrm{c}} - E_\mathrm{J0}\left(1 - \cos\varphi - j\varphi\right) , \tag{1.10}$$

where $E_\mathrm{c} = (2e)^2/2C$ is the charging energy of the capacitor with the charge of one Cooper pair and $K(\dot{\varphi})$ is the kinetic energy corresponding to the first term on the left hand side of Eq. (1.9). The equation of motion can be obtained from the Lagrangian as

$$\frac{d}{dt}\frac{\partial \mathcal{L}}{\partial \dot{\varphi}} - \frac{\partial \mathcal{L}}{\partial \varphi} = 0 \,. \tag{1.11}$$

We note that Eqs. (1.9) and (1.10) are a quasi-classical description of the Josephson junction dynamics. They describe the classical motion of a phase particle in the tilted washboard potential. For a description of superconducting qubits based on Josephson junctions, a full quantum mechanical description of the Josephson junctions is required. As mentioned above, this occurs when the charging energy becomes comparable with the Josephson energy, $E_\mathrm{C} \sim E_\mathrm{J}$, respectively, $N \sim 1$. In this situation, the Josephson phase difference φ stops being a good quantum number and we have to consider the commutation relation between the corresponding phase operator $\hat{\varphi}$ and charge operator $\hat{Q}$ [7]. Depending on the relative magnitude of the Josephson energy E_J and the charging energy E_c, one obtains different types of superconducting qubits [8]. For the Josephson junctions used in the JPAs presented here, the Josephson energy strongly dominates over the charging energy, $E_\mathrm{J}/E_\mathrm{c} \simeq 10^3$. Furthermore, the Josephson nonlinearity in JPAs is diluted by galvanically connecting the Josephson junctions to a coplanar waveguide resonator. Consequently, the dynamics of the phase difference $\hat{\varphi}$ can be well described with the above quasi-classical model, and the charging energy of the Josephson junction and any uncertainty between the charge and phase degree of freedom can be neglected.

Task 1: Josephson junctions

Would it be possible to build a superconducting Josephson junction working at room temperatures? Consider your knowledge regarding the fundamental terms: superconducting critical temperature T_c, Cooper pairs, Meißner-Ochsenfeld effect, flux quantum, Josephson contact, Josephson equations.

Task 2: Tilted washboard potential

Draw the potential energy of a lumped Josephson junction as a function of the Josephson phase difference. How does this potential change when one increases the bias current through the Josephson junction?

Task 3: Conjugate variables

What are the conjugate variables relevant to Josephson junctions? Which physical parameters define the corresponding regimes?

1.2 Dc-SQUID

A central building block of the JPA is a direct current superconducting quantum interference device (dc-SQUID). It consists of two Josephson junctions with critical currents I_c in a superconducting loop, as shown in Fig. 1.1 (b). For simplicity, we assume equal critical currents of the Josephson junctions but different I_c are also possible. An externally applied magnetic field $\mathbf{B}$ causes a magnetic flux Φ_ext through the loop. Due to boundary conditions, the total phase change along a closed contour C around the dc-SQUID loop is fixed to $\oint_C \nabla\theta = 2\pi n$ with $n \in Z_0$. By using the gauge invariant phase difference in Eq. (1.1) and the phase gradient in the bulk superconductor, we can write [4]

$$\nabla\theta = \frac{2\pi}{\Phi_0}(\Lambda\mathbf{J}_s + \mathbf{A})\,, \tag{1.12}$$

where $\mathbf{J}_s$ is the supercurrent density, $\mathbf{A}$ is the vector potential and Λ is the London parameter. For simplicity, we choose an integration path inside the bulk superconductor where the supercurrent density $\mathbf{J}_s$ is approximately zero and obtain

$$\varphi_2 - \varphi_1 = \frac{2\pi\Phi}{\Phi_0} + 2\pi n\,. \tag{1.13}$$

This equation provides us with a connection between the phase differences $\varphi_{1,2}$ across the Josephson junctions and the total magnetic flux Φ threading the loop. The total magnetic flux $\Phi = \Phi_\mathrm{ext} + L_\mathrm{loop}I_\mathrm{circ}$ consists of the externally applied flux Φ_ext and the self-induced flux $L_\mathrm{loop}I_\mathrm{circ}$, where L_loop is the self-inductance of the superconducting loop. The circulating current is given by

$$I_\mathrm{circ} = \frac{I_1 - I_2}{2} = I_\mathrm{c}\cos\left(\frac{\varphi_1+\varphi_2}{2}\right)\sin\left(\frac{\varphi_1-\varphi_2}{2}\right) = -I_\mathrm{c}\cos\varphi_+\sin\varphi_-\,, \tag{1.14}$$

where we introduced new phase differences

$$\varphi_+ \equiv \frac{\varphi_1+\varphi_2}{2} \qquad \text{and} \qquad \varphi_- \equiv \frac{\varphi_2-\varphi_1}{2}\,, \tag{1.15}$$

in order to simplify the notation. For example, the fluxoid quantization condition in terms of the new phase difference φ_- reads

$$\varphi_- = \pi \frac{\Phi}{\Phi_0} + \pi n \,. \tag{1.16}$$

Here, it is useful to define the total transport current through the dc-SQUID

$$I_{\mathrm{tr}} = I_1 + I_2 = 2I_{\mathrm{c}} \sin\left(\frac{\varphi_1 + \varphi_2}{2}\right) \cos\left(\frac{\varphi_1 - \varphi_2}{2}\right) = 2I_{\mathrm{c}} \sin\varphi_+ \cos\varphi_- \,, \tag{1.17}$$

which is given by the sum of the currents through each Josephson junction. The screening properties of the superconducting loop are summarized in the so-called screening parameter [9]

$$\beta_{\mathrm{L}} \equiv \frac{2L_{\mathrm{loop}} I_{\mathrm{c}}}{\Phi_0} \,, \tag{1.18}$$

which relates the maximally induced flux $L_{\mathrm{loop}} I_{\mathrm{c}}$ to half of a flux quantum $\Phi_0/2$. With the above equations we can write the total flux through the dc-SQUID loop as

$$\frac{\Phi}{\Phi_0} = \frac{\Phi_{\mathrm{ext}}}{\Phi_0} - \frac{\beta_{\mathrm{L}}}{2} \cos\varphi_+ \sin\varphi_- \,, \tag{1.19}$$

If we now consider the limiting case $\beta_{\mathrm{L}} \simeq 0$, the self-induced flux by the dc-SQUID can be neglected and, consequently, the total flux can be approximated by the externally applied flux, $\Phi \approx \Phi_{\mathrm{ext}}$. Then, in analogy to the critical current of a Josephson junction, one can define a maximum transport current of the dc-SQUID [5]

$$I_{\mathrm{s}}^{\max}(\Phi_{\mathrm{ext}}) = 2I_{\mathrm{c}} \left| \cos\left(\pi \frac{\Phi_{\mathrm{ext}}}{\Phi_0}\right) \right| \,. \tag{1.20}$$

Consequently, for $\beta_{\mathrm{L}} \simeq 0$, the dc-SQUID can be considered as a single Josephson junction with a flux-modulated maximum supercurrent and, thus, in analogy to Eq. (1.5), a flux-tunable inductance of the dc-SQUID can be defined as [10]

$$L_{\mathrm{s}}(\Phi_{\mathrm{ext}}) = \frac{\Phi_0}{2\pi I_{\mathrm{s}}^{\max}} = \frac{\Phi_0}{4\pi I_{\mathrm{c}} \left| \cos\left(\pi \frac{\Phi_{\mathrm{ext}}}{\Phi_0}\right) \right|} \,. \tag{1.21}$$

This equation nicely illustrates that the dc-SQUID can be applied both as an in-situ flux-tunable inductance as well as a nonlinear element in superconducting circuits.

For the case $\beta_{\mathrm{L}} > 0$, the self-inductance of the loop can no longer be neglected. Therefore, the behavior of the dc-SQUID is described by Eqs. (1.17) and (1.19). These two equations need to be solved self-consistently under the constraint of the fluxoid quantization condition in Eq. (1.13). For general cases, it is not possible to obtain an analytic expression but nevertheless one can define

$$I_{\mathrm{s}}^{\max}(\Phi_{\mathrm{ext}}) = 2I_{\mathrm{c}} \cdot j_{\mathrm{c}}(\Phi_{\mathrm{ext}})\,, \tag{1.22}$$

$$L_{\mathrm{s}}(\Phi_{\mathrm{ext}}) = \frac{\Phi_0}{4\pi I_{\mathrm{c}} \cdot j_{\mathrm{c}}(\Phi_{\mathrm{ext}})}\,, \tag{1.23}$$

where $j_{\mathrm{c}}(\Phi_{\mathrm{ext}})$ is a dimensionless critical supercurrent through the dc-SQUID. We refer the reader to Sec. 1.4 for a detailed discussion on how we simulate and use $j_{\mathrm{c}}(\Phi_{\mathrm{ext}})$ in order to describe the flux dependence of a coplanar waveguide resonator short-circuited to ground by a dc-SQUID.

Similarly to the case of a single Josephson junction, one can write Kirchhoff's law for both junctions [5]

$$\frac{\ddot{\varphi}_1}{\omega_{\mathrm{p1}}^2} + \frac{\dot{\varphi}_1}{\omega_{\mathrm{c1}}} = -\sin\varphi_1 + j_{\mathrm{tr}} + \frac{1}{\pi\beta_{\mathrm{L}}}\left(\varphi_2 - \varphi_1 - 2\pi\frac{\Phi_{\mathrm{ext}}}{\Phi_0}\right)\,, \tag{1.24}$$

$$\frac{\ddot{\varphi}_2}{\omega_{\mathrm{p2}}^2} + \frac{\dot{\varphi}_2}{\omega_{\mathrm{c2}}} = -\sin\varphi_2 + j_{\mathrm{tr}} - \frac{1}{\pi\beta_{\mathrm{L}}}\left(\varphi_2 - \varphi_1 - 2\pi\frac{\Phi_{\mathrm{ext}}}{\Phi_0}\right)\,, \tag{1.25}$$

where indices 1 and 2 denote the two Josephson junctions and $j_{\mathrm{tr}} = I_{\mathrm{tr}}/(2I_{\mathrm{c}})$. Finally, we neglected the dissipative terms and define the Lagrangian of a dc-SQUID [11]

$$\mathcal{L} = \frac{\hbar^2}{4E_{\mathrm{c}}}(\dot{\varphi}_1^2+\dot{\varphi}_2^2) - E_{\mathrm{J0}}\left(2 - \cos\varphi_1 - \cos\varphi_2 - j_{\mathrm{tr}}(\varphi_1+\varphi_2)\right) - \frac{E_{\mathrm{J0}}}{2\pi\beta_{\mathrm{L}}}\left(\varphi_2 - \varphi_1 - 2\pi\frac{\Phi_{\mathrm{ext}}}{\Phi_0}\right)^2\,, \tag{1.26}$$

which can also be written in the form

$$\mathcal{L} = \frac{\hbar^2}{2E_{\mathrm{c}}}(\dot{\varphi}_+^2+\dot{\varphi}_-^2) - E_{\mathrm{J0}}\left(2 - 2\cos\varphi_+\cos\varphi_- - 2j_{\mathrm{tr}}\varphi_+\right) - \frac{2E_{\mathrm{J0}}}{\pi\beta_{\mathrm{L}}}\left(\varphi_- - \pi\frac{\Phi_{\mathrm{ext}}}{\Phi_0}\right)^2\,. \tag{1.27}$$

Task 4: Flux-tunable dc-SQUID

Sketch a flux dependence of the maximum Josephson supercurrent through a dc-SQUID.

Task 5: Screening parameter

What is the physical meaning of the screening parameter β_L?

1.3 Coplanar waveguide resonators

In circuit quantum electrodynamics, superconducting resonators have various purposes. For example, they can serve as quantum bus [12], quantum memory [13], or can be

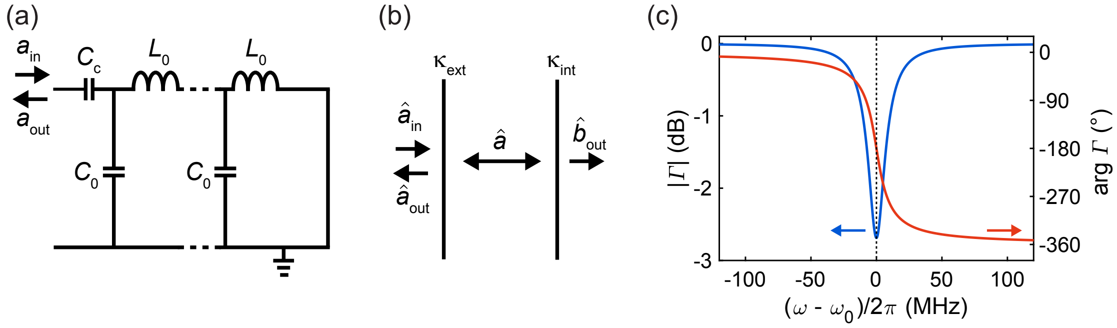

Figure 1.2: (a) Distributed element model of a CPW resonator. This resonator can be described as a CPW transmission line with the length l which is short-circuited to ground at one end, creating a voltage node (current anti-node). Such resonator configuration corresponds to the $\lambda/4$-type. Here, L_0 and C_0 are the inductance and capacitance per unit length, and C_c is a coupling capacitance which allows an input signal a_{in} to enter and a signal a_{out} to leave the resonator. (b) Input-output model of a resonator with an internal mode $\hat{a}$ and internal loss rate κ_{int} which couples to a loss mode $\hat{b}_{out}$. Input-output coupling is expressed by an external coupling rate κ_{ext}. The operators $\hat{a}_{in}$, $\hat{a}_{out}$, $\hat{a}$, and $\hat{b}_{out}$ are treated quantum-mechanically. (c) Reflection magnitude $|\Gamma|$ and reflection angle Arg(Γ) versus readout frequency for $Q_{ext} = 300$, $Q_{int} = 1000$ and $\omega_0/2\pi = 5\,\text{GHz}$.

applied to study fundamental light-matter interactions [14]. Furthermore, they are an essential part of JPAs.

First, we consider a coplanar waveguide (CPW) which acts as a quasi one-dimensional transmission line. Since we are interested in frequencies in the gigahertz regime, the lateral dimensions of the CPW should be on the order of the corresponding wavelength, i.e. on the order of a few millimeters. Therefore, the CPW needs to be described with a distributed element model, where each circuit element is considered to be infinitesimally small. The wave propagation through such a system is generally described by the telegrapher's equations [15]. Since our CPW structures consist of a superconducting material, we can approximate the CPW with a lossless transmission line with a characteristic impedance [15]

$$Z = \sqrt{\frac{L_0}{C_0}}\,, \tag{1.28}$$

where L_0 and C_0 are the inductance and capacitance per unit length of the transmission line, respectively. In general, disregarding polarization, an infinite homogeneous transmission line does not have any mode restrictions due to the absence of boundary conditions.

In order to create a resonant structure, one needs to apply boundary conditions to the waves propagating through the transmission line. One way to realize such a boundary condition is to create a discontinuity in the transmission line by introducing a line break with a corresponding capacitance C_c. Simultaneously, this capacitor acts as an external port to couple to the field inside the resonator. Alternatively, one can short-circuit the CPW to ground which creates a voltage node and current antinode. We focus on quarter-wavelength resonators where both of these boundary conditions are employed, namely, a coupling capacitance at one end of the resonator and a short to ground at the other end as shown in Fig. 1.2 (a). The fundamental resonance frequency of a quarter-wavelength resonator with length l is given by [16]

$$f_\mathrm{r} = \frac{c}{\sqrt{\epsilon_\mathrm{eff}}}\frac{1}{4l} = \frac{1}{4l\sqrt{L_0 C_0}}\,, \tag{1.29}$$

where $\epsilon_\mathrm{eff} = c^2/v_\mathrm{ph}^2$ is the effective permittivity of the CPW, c is the velocity of light in vacuum and $v_\mathrm{ph} = 1/\sqrt{L_0 C_0}$ is the phase velocity. The length of the resonator is connected to the wavelength of the fundamental mode as $l = \lambda/4$, hence the name quarter-wavelength resonator.

In order to probe the resonator, a microwave tone is applied and the reflected signal from the resonator is measured as depicted in Fig. 1.2 (b,c). The reflected signal can differ in amplitude and phase from the applied signal which is captured by the complex reflection coefficient [17]

$$\Gamma = \frac{(\omega-\omega_0)^2 + i\kappa_\mathrm{int}(\omega-\omega_0) + (\kappa_\mathrm{ext}^2 - \kappa_\mathrm{int}^2)/4}{[(\omega-\omega_0) + i(\kappa_\mathrm{ext}+\kappa_\mathrm{int})/2]^2}\,, \tag{1.30}$$

which is calculated using an input-output formalism. Here, κ_int and κ_ext are the internal and external loss rates, respectively, and ω_0 is the resonance frequency of the resonator in angular units.

The loss rates are related to the quality factor Q of the resonator, which is an important quantity characterizing its performance. The quality factor is defined as [15]

$$Q = 2\pi\frac{\text{average energy stored}}{\text{energy loss/cycle}} = \frac{\omega_0}{\kappa_\mathrm{tot}}\,, \tag{1.31}$$

where $\kappa_\mathrm{tot} = \kappa_\mathrm{int} + \kappa_\mathrm{ext}$ defines the total loss rate. Consequently, the loaded quality factor Q_l is defined by the sum of loss rates

$$\frac{1}{Q_\mathrm{l}} = \frac{1}{Q_\mathrm{int}} + \frac{1}{Q_\mathrm{ext}} = \frac{\kappa_\mathrm{int}+\kappa_\mathrm{ext}}{\omega_0}\,, \tag{1.32}$$

where $Q_\mathrm{int} = \omega_0/\kappa_\mathrm{int}$ and $Q_\mathrm{ext} = \omega_0/\kappa_\mathrm{ext}$ are the internal and external quality factor, respectively. The external loss rate is mainly defined by the coupling capacitance and determines how well a probe tone couples to the resonator. The internal loss rate is a sum of various, typically unwanted, loss mechanisms such as losses from two-level fluctuators [18], surface resistance [19], or radiation losses.

Task 6: Resonator

How to design a coplanar waveguide resonator for a given f_r? How to design the corresponding quality factors?

1.4 Resonance frequency of the JPA

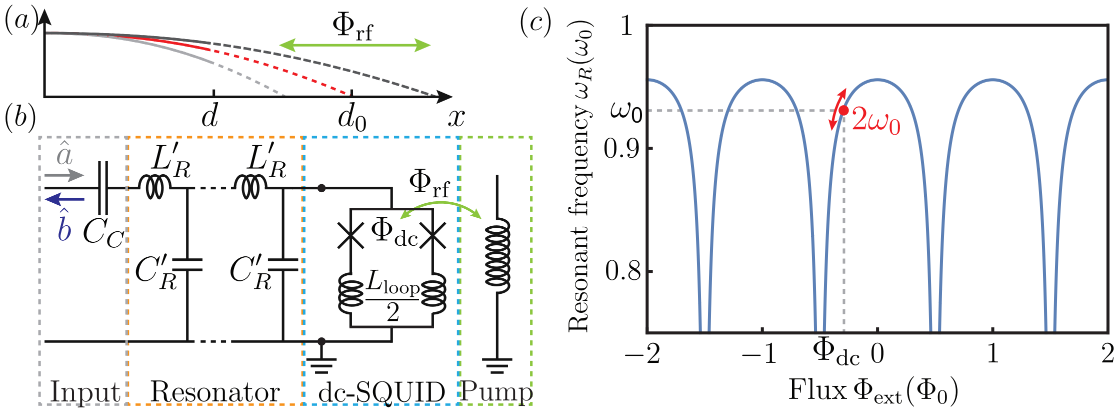

Figure 1.3: (a) Change of effective length of resonator to illustrate the change of resonance frequency due to the magnetic flux modulation through a dc-SQUID. (b) Circuit diagram of a flux-driven JPA consisting of an input capacitance (grey), CPW resonator (orange), dc-SQUID (blue), and pump line (green). (c) Resonance frequency vs. externally applied flux. A constant magnetic flux Φ_{dc} fixes the working point at a frequency ω_0.

We now consider the flux-driven JPA [20] consisting of a quarter-wavelength CPW resonator, which is short-circuited to ground by a dc-SQUID (see Fig. 1.3). Here, the dc-SQUID acts as a flux-tunable nonlinear inductor which contributes to the quasi-static resonance frequency ω_0 of the JPA. As discussed in Sec. 1.2, we can use a magnetic flux to tune the dc-SQUID inductance and, in this way, the resonance frequency of the whole JPA circuit. In order to induce parametric effects, an on-chip antenna couples inductively to the dc-SQUID loop via the loop inductance L_{loop} and is used to apply a strong coherent pump tone with an angular frequency $\omega_{\mathrm{p}} = 2\omega_0$.

In the following, we discuss how the resonance frequency of the JPA circuit depends on an external magnetic flux Φ_{ext} threading the dc-SQUID loop. The treatment is applicable for arbitrary flux-screening of the dc-SQUID which can be quantified by the dimensionless screening parameter β_{L}, as defined in Eq. (1.18). Based on the distributed element model for the quarter-wavelength resonator and a lumped element model for the dc-SQUID (see Fig. 1.3), one arrives at a transcendental equation for the resonance frequency ω_0 of the JPA [21, 22, 23]

$$\frac{\pi\omega_0}{2\omega_\mathrm{r}}\tan\left(\frac{\pi\omega_0}{2\omega_\mathrm{r}}\right)=\frac{(2\pi)^2}{\Phi_0^2}L_\mathrm{r}E_s(\Phi_\mathrm{ext})-\frac{2C_\mathrm{s}}{C_\mathrm{r}}\left(\frac{\pi\omega_0}{2\omega_\mathrm{r}}\right)^2. \tag{1.33}$$

Here, L_r, C_r, and $\omega_\mathrm{r}/2\pi$ are the total inductance, the total capacitance and the resonance frequency of the bare resonator, respectively, $E_\mathrm{s}(\Phi_\mathrm{ext})$ is the flux-dependent potential energy of the dc-SQUID as defined below, and C_s is the capacitance of one Josephson junction. For the presented samples, the last term in Eq. (1.33) can be neglected, since the capacitance of the Josephson junctions is much smaller than the one of the resonator, $C_\mathrm{s} \ll C_\mathrm{r}$. For a vanishing transport current I_tr through the dc-SQUID, the normalized critical supercurrent $j_\mathrm{c}(\Phi_\mathrm{ext})$, used in Eqs. (1.22) and (1.23), only depends on φ_- and can be simplified to

$$j_\mathrm{c}=|\cos\varphi_-^\mathrm{min}(\Phi_\mathrm{ext})|\,, \tag{1.34}$$

where $\varphi_\pm \equiv (\varphi_1 \pm \varphi_2)/2$ are defined in Eq. (1.15). The superscript in $\varphi_\pm^\mathrm{min}(\Phi_\mathrm{ext})$ denotes the steady-state phase differences for a given external flux Φ_ext. Thus, the Josephson inductance of the dc-SQUID reads

$$L_\mathrm{s}(\Phi_\mathrm{ext})=\frac{\Phi_0}{4\pi I_\mathrm{c}|\cos\varphi_-^\mathrm{min}(\Phi_\mathrm{ext})|}\,, \tag{1.35}$$

where I_c is the critical current of a single Josephson junction. Using L_s, we can express the flux-dependent energy of the dc-SQUID as

$$E_\mathrm{s}(\Phi_\mathrm{ext})=\frac{\Phi_0^2}{(2\pi)^2}\frac{1}{L_\mathrm{s}(\Phi_\mathrm{ext})+L_\mathrm{loop}/4}\,, \tag{1.36}$$

where the non-zero dc-SQUID loop inductance L_loop is split between both arms of the dc-SQUID [24].

The tangent in Eq. (1.33) can be expanded into a Laurent series near $\pi/2$ for $\omega_0/\omega_\mathrm{r} \simeq 1$. Consequently, we obtain a simplified expression for the resonance frequency of the JPA in terms of inductances

$$\omega_0(\Phi_\mathrm{ext})=\omega_\mathrm{r}\left[1+\frac{L_\mathrm{s}(\Phi_\mathrm{ext})+L_\mathrm{loop}/4}{L_\mathrm{r}}\right]^{-1}. \tag{1.37}$$

We now discuss the effect of flux-screening of the dc-SQUID depending on the screening parameter β_L. In general, $\varphi_-^\mathrm{min}(\Phi_\mathrm{ext})$ exhibits a non-trivial dependence on the external magnetic flux. According to the fluxoid quantization, $\varphi_-^\mathrm{min}(\Phi_\mathrm{ext})$ is related to the total flux $\Phi = \Phi_\mathrm{ext} + L_\mathrm{loop}I_\mathrm{circ}$ threading the dc-SQUID according to $\varphi_-^\mathrm{min} = \pi(\Phi/\Phi_0)$. As already discussed in Sec. 1.2, we have $\Phi \approx \Phi_\mathrm{ext}$ in the case of a vanishing screening parameter $\beta_\mathrm{L} \simeq 0$. In this case, the phase of one Josephson junction relative to the other one is fixed by the fluxoid quantization, reducing the available degrees of freedom from two to one. This results in a single-valued dependence $\varphi_-^\mathrm{min} = \pi(\Phi_\mathrm{ext}/\Phi_0)$. A mechanical analog of this situation are two strongly coupled pendula, where the system can be described by a single deflection angle, i.e., a single degree of freedom due to the rigid coupling. However, if the screening parameter β_L becomes non-zero, there is no analytic expression for $\varphi_-^\mathrm{min}(\Phi_\mathrm{ext})$ anymore and the dependence has to be calculated numerically. Consequently, the JPA resonance frequency can exhibit a non-trivial behavior when varying the external flux.

Task 7: Bonus – Critical coupling

We have considered external and internal quality factors Q_ext, Q_int. When would the JPA resonator become critically coupled? If in doubt, refer to the general resonator theory for the latter question. How could it be possible to achieve critical coupling in the case of a flux-tunable JPA?

1.5 Parametric amplification with flux-driven JPAs

In general, amplification in nonlinear resonators can be enabled by driving a parametric process with an external pump tone. The pump tone must very one of the parameters of this resonator, such as inductance L or capacitance C, in a periodic fashion which gives rise to parametric effects [25, 26]. In order for such processes to happen, the resonator requires a nonlinear element. For superconducting circuits, Josephson junctions are routinely used for this purpose and a variety of parametric amplifiers have been realized based on them [27, 28, 29, 30, 31, 32, 33]. We focus on flux-driven JPAs [20] where the pump tone is inductively coupled to the JPA and has a frequency ω_p of twice the resonance frequency of the circuit. Here, the pump tone leads to a periodic modulation of the dc-SQUID inductance which, in turn, causes a periodic modulation of the resonance frequency ω_0 of the JPA circuit. Consequently, the induced parametric modulation enables a three-wave mixing process where an incident signal mode at frequency $\omega_\mathrm{s} = \omega_\mathrm{p}/2 + \delta\omega$ and detuning $\delta\omega$ is amplified, as depicted in Fig. 1.4. At the same time, an idler mode at frequency $\omega_\mathrm{i} = \omega_\mathrm{p}/2 - \delta\omega$ is created. One can imagine this process as a pump photon splitting into one signal photon and one idler photon such that the energy is conserved, $\omega_\mathrm{p} = \omega_\mathrm{s} + \omega_\mathrm{i}$ [34].

In order to describe the flux-driven JPA analytically, we employ an input-output model for the JPA developed by Yamamoto *et al.* [17] and start with an unperturbed classical harmonic oscillator whose resonance frequency ω_0 is periodically modulated such that $\omega_0 \to \omega_0\,[1 + \epsilon/2\cos(\alpha\omega_0 t)]$, where $\epsilon/2$ and $\alpha\omega_0$ are the amplitude and frequency of the modulation, respectively. Consequently, the classical equation of motion reads [17]

$$\frac{d^2x}{dt^2} + \omega_0^2\,[1 + \epsilon\cos(\alpha\omega_0 t)]\,x = 0\,. \tag{1.38}$$

Here, we neglected the ϵ^2 term since we only consider small modulation amplitudes, i.e., small pump amplitudes. In a quantum-mechanical picture, the corresponding Hamilto-

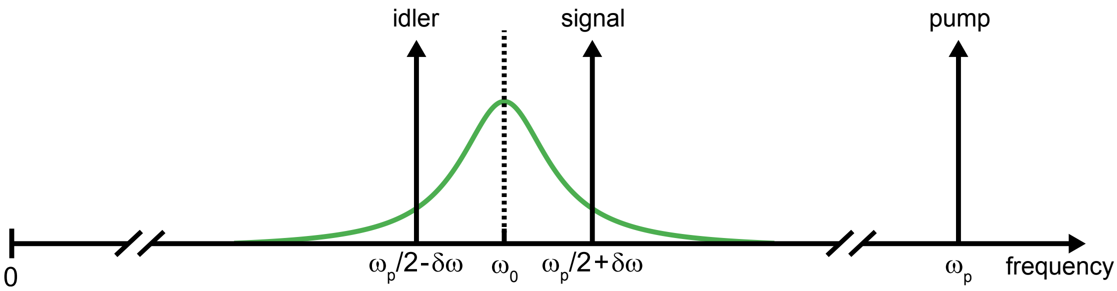

Figure 1.4: Scheme of relevant frequencies for parametric amplification with a flux-driven JPA. The pump frequency ω_p is at roughly twice the JPA resonance frequency ω_0. The signal mode at frequency $\omega_\mathrm{p}/2+\delta\omega$ is amplified and an idler mode at frequency $\omega_\mathrm{p}/2-\delta\omega$ is created.

nian in terms of the annihilation and creation operators reads

$$H = \hbar\omega_0 \left[\hat{a}^\dagger\hat{a} + \frac{1}{2} + \epsilon\cos(\alpha\omega_0 t)(\hat{a}+\hat{a}^\dagger)^2\right] . \tag{1.39}$$

After introducing a signal port and a loss port to the Hamiltonian, the Heisenberg equation of motion for the resonator field $\hat{a}$ can be solved in a frame rotating with $\alpha\omega_0/2$ and one obtains expressions for the output field of the JPA. For details on the derivation, we refer the reader to Ref. [17]. We only consider the case where the applied pump tone is twice the resonance frequency of the JPA, $\omega_\mathrm{p} = 2\omega_0$, corresponding to $\alpha = 2$. One can differentiate between two operation modes of the JPA which are discussed in the following.

Task 8: Working point

Where would you expect is an optimal working point of a flux-driven JPA? Explain your choice.

Task 9: Signal mixing

Define signal, idler, and pump modes in a flux-driven JPA. What is the relation between these modes?

Nondegenerate gain

The JPA is operated in the nondegenerate operation mode if the input signal at frequency $\omega_\mathrm{s} = \omega_\mathrm{p}/2 + \delta\omega$ has a non-zero offset to half the pump frequency, $\delta\omega \neq 0$. In the nondegenerate operation mode, both electromagnetic quadratures of the signal, are amplified equally. Therefore, the JPA acts as a phase-preserving amplifier. In this context, relation $S = S_0\cos(\omega_\mathrm{s}t+\phi) = P\cos\omega_\mathrm{s}t + Q\sin\omega_\mathrm{s}t$ establishes the connection between the signal quadratures, P and Q, and the corresponding signal amplitude S_0 and phase

ϕ. The interpretation of electromagnetic signals in terms of field quadratures is often used in classical microwave engineering. Additionally, this approach is very useful for describing quantum signals, where the corresponding quantum-mechanical quadrature operators do not have deep internal mathematical problems in contrast to various forms of phase operators (see Ref. [35] for more details).

For a flux-driven JPA, we can write explicit expressions for the signal and idler power gain as [17]

$$G_{\mathrm{s}}(\delta\omega) = \frac{\kappa_{\mathrm{int}}^2 \delta\omega^2 + \left[(\kappa_{\mathrm{int}}^2 - \kappa_{\mathrm{ext}}^2)/4 - \epsilon^2\omega_0^2 - \delta\omega^2\right]^2}{\kappa_{\mathrm{tot}}^2 \delta\omega^2 + \left[\kappa_{\mathrm{tot}}^2/4 - \epsilon^2\omega_0^2 - \delta\omega^2\right]^2}\,, \tag{1.40}$$

$$G_{\mathrm{i}}(\delta\omega) = \frac{\kappa_{\mathrm{ext}}^2 \epsilon^2 \omega_0^2}{\kappa_{\mathrm{tot}}^2 \delta\omega^2 + \left[\kappa_{\mathrm{tot}}^2/4 - \epsilon^2\omega_0^2 - \delta\omega^2\right]^2}\,, \tag{1.41}$$

where $\kappa_{\mathrm{tot}} = \kappa_{\mathrm{ext}} + \kappa_{\mathrm{int}}$ is the sum of external and internal loss rates. Equations (1.40) and (1.41) are only valid for modulation amplitudes below a certain the threshold value $\epsilon \leq \epsilon_{\mathrm{c}} = \kappa_{\mathrm{tot}}/2\omega_0$. Above this threshold, the JPA acts as a Josephson parametric phase-locked oscillator, where two dynamical coherent states exist inside the oscillator [17]. The threshold appears, similar to a driven Duffing oscillator, because multiple stable states exist for a highly-driven JPA [22]. For vanishing internal losses, $\kappa_{\mathrm{int}} = 0$, we obtain the relation $G_{\mathrm{s}}(\delta\omega) - G_{\mathrm{i}}(\delta\omega) = 1$.

JPAs are routinely used as low-noise amplifiers of microwave signals in the gigahertz regime, since they provide an excellent noise performance [36, 37, 38, 39]. According to the Haus-Caves theorem [40, 41], phase-preserving amplifiers possess a lower limit on the noise they add to the amplified signal. In order to provide a universal measure between amplifiers of different nature, the noise performance of various amplifiers is often expressed in terms of extra added noise photons A referred to the input. The minimum number of added noise photons is limited by [41]

$$A \geq \frac{1}{2}\left|1 - \frac{1}{G_{\mathrm{s}}}\right|\,. \tag{1.42}$$

Consequently, for $G_{\mathrm{s}} \gg 1$, a phase-preserving amplifier adds at least half of a noise photon to the input signal, what is known as the standard quantum limit for phase-insensitive amplification. From a theoretical point of view, this fundamental limit originates from the fact that the bosonic commutation relation of the amplified mode needs to be fulfilled [28]. The physical origin of the added noise consists in the admixture of the idler mode to the signal mode. During the parametric amplification, the noise at the idler frequency $\omega_{\mathrm{i}} = \omega_{\mathrm{p}}/2 - \delta\omega$ is converted to the signal frequency ω_{s}, where it is combined with the amplified original signal [34]. The limit of at least half of an added noise photon is attributed to the noise floor of the idler mode limited by the quantum fluctuations.

Task 10: Standard quantum limit

What is the standard quantum limit (SQL) of for phase-insensitive amplification?

What is the physical origin of the SQL? Can the JPA achieve this limit?

Additional topic: degenerate gain

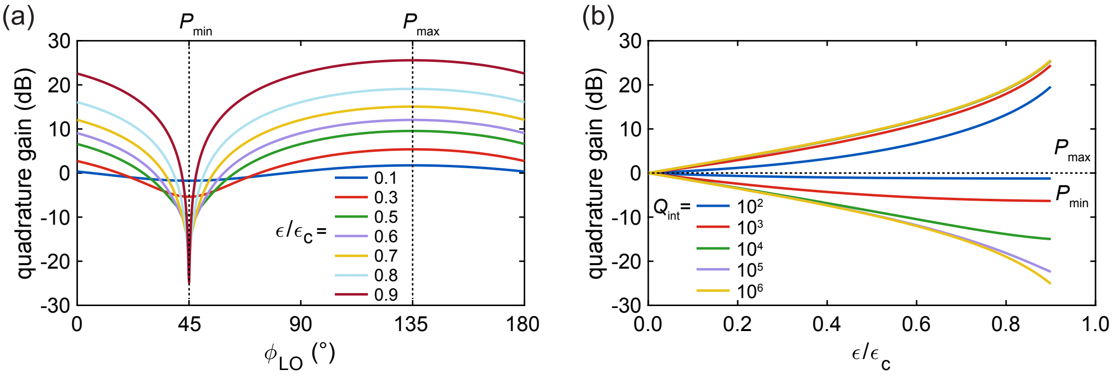

Figure 1.5: (a) Quadrature gain P as a function of the local oscillator phase ϕ_{LO} for different modulation amplitudes $\epsilon/\epsilon_{\mathrm{c}}$ and $Q_{\mathrm{int}} = 1 \cdot 10^6$. (b) Maximum gain $P_{\max}$ and minimum gain $P_{\min}$ as a function of the modulation amplitude $\epsilon/\epsilon_{\mathrm{c}}$ for different internal quality factors Q_{int}. Both panels are calculated with $Q_{\mathrm{ext}} = 300$ and $\omega_0/2\pi = 5\,\mathrm{GHz}$.

We now consider the case where half the pump frequency and the signal frequency are degenerate, $\omega_{\mathrm{s}} = \omega_{\mathrm{p}}/2$, which implies $\delta\omega = 0$. In this scenario, the signal and idler modes have the same frequencies which allows them to interfere with a fixed phase relation. This results in a phase-sensitive amplification where different quadratures are amplified with different gains [28]. For our case of flux-driven JPAs, the degenerate signal gain depends on the phase θ between the pump and the microwave signal and is given by [17]

$$G_{\mathrm{d}}(\theta) = \frac{\left(\frac{\kappa_{\mathrm{ext}}^2 - \kappa_{\mathrm{int}}^2}{4} + \epsilon^2\omega_0^2\right)^2 + \epsilon^2\kappa_{\mathrm{ext}}^2\omega_0^2 - 2\epsilon\kappa_{\mathrm{ext}}\omega_0\left(\frac{\kappa_{\mathrm{ext}}^2 - \kappa_{\mathrm{int}}^2}{4} + 4\delta^2\omega_0^2\right)\sin(2\theta)}{\left(\frac{\kappa^2}{4} - \epsilon^2\omega_0^2\right)^2}. \quad (1.43)$$

The latter equation is again only valid below the threshold $\epsilon \leq \epsilon_{\mathrm{c}}$. If we assume an overcoupled JPA, $\kappa_{\mathrm{ext}} > \kappa_{\mathrm{int}}$, or more precisely $(\kappa_{\mathrm{ext}}^2 - \kappa_{\mathrm{int}}^2)/4 + \epsilon^2\omega_0^2 > 0$, we can define the minimum and maximum degenerate gains

$$G_{\mathrm{d}}^{\min} = \left(\frac{\epsilon\omega_0 - (\kappa_{\mathrm{ext}} - \kappa_{\mathrm{int}})/2}{\epsilon\omega_0 + (\kappa_{\mathrm{ext}} + \kappa_{\mathrm{int}})/2}\right)^2, \quad (1.44)$$

$$G_{\mathrm{d}}^{\max} = \left(\frac{\epsilon\omega_0 + (\kappa_{\mathrm{ext}} - \kappa_{\mathrm{int}})/2}{\epsilon\omega_0 - (\kappa_{\mathrm{ext}} + \kappa_{\mathrm{int}})/2}\right)^2, \quad (1.45)$$

for $\theta^{\min} = \pi/4 + n\pi$ and $\theta^{\max} = 3\pi/4 + n\pi$, respectively. The difference between the phases is $\pi/2$ which means that the maximally amplified and deamplified quadratures are orthogonal to each other. Furthermore, without any internal losses, $\kappa_{\text{int}} = 0$, we obtain

$$G_{\text{d}}^{\text{min}}\, G_{\text{d}}^{\text{max}} = 1\,. \tag{1.46}$$

In the phase-sensitive regime, JPAs allow for amplification without adding any additional noise to the signal according to the Haus-Caves theorem. In fact, for a phase-sensitive amplifier, different amounts of noise can be added to each quadrature [41]

$$A_1 A_2 \geq \frac{1}{16}\left|1 - \frac{1}{\sqrt{G_1 G_2}}\right|^2\,, \tag{1.47}$$

where A_1 and A_2 denote the added noise photons in orthogonal quadratures with respective gains G_1 and G_2. If we consider an amplifier for which one quadrature is amplified ($G_1 > 1$) while the orthogonal quadrature is deamplified ($G_2 < 1$), the added noise can be zero under the condition $G_1 G_2 = 1$. According to Eq. (1.46), JPAs can reach this limit in the absence of internal losses. In fact, it has been experimentally demonstrated that JPAs can phase-sensitively amplify weak microwave signals with a noise performance below the standard quantum limit [42, 43, 28].

Task 11: Bonus – Degenerate and nondegenerate gain

Briefly explain the difference between the degenerate and nondegenerate amplification regimes.

1.6 Additional topic: squeezing with flux-driven JPAs

In the last subsection, we discussed how JPAs can be used as nondegenerate and degenerate amplifiers of microwave signals. In addition, JPAs can also be employed as a tool to generate quantum signals in the form of squeezed states (see Fig. 1.6). From the well-known definition of single-mode squeezed (SMS) states in quantum optics [44], we know that the variance along different quadrature directions varies for SMS states. In this sense, single-mode squeezing of the JPA is closely connected to the degenerate operation mode of the JPA. In order to obtain expressions for the variances of a squeezed state produced by a flux-driven JPA, we assume a fictional homodyne setup depicted in Fig. 1.7. The demonstrated down-conversion scheme is very important for the squeezed states detection and tomography because typical characteristics frequencies of these states are in the range of $5 - 10\,\text{GHz}$. Such high-frequency signals are difficult to directly detect (digitize) even the best analog-to-digital converters (ADCs) due to technical limitations of digitization rates. Modern ADCs typically have these rates in the range of 100 MHz - 1 GHz. Therefore, a more conventional approach is to convert high-frequency signals to the low-frequency range of several tens of MHz (or lower), where the signal detection and digitization is easily possible. In Fig. 1.7, the squeezed signal from the JPA is sent to a mixer which is driven by a local oscillator (LO) with frequency $\omega_{\text{p}}/2$ and

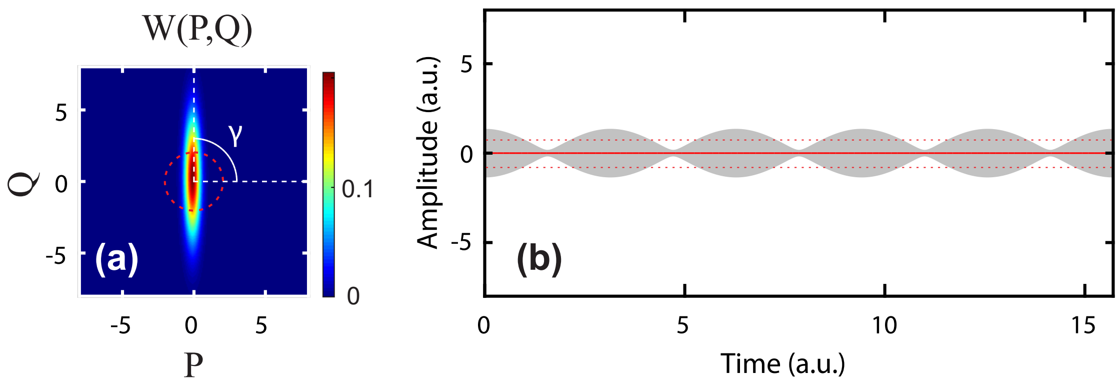

Figure 1.6: Illustration of propagating squeezed vacuum states. Plot **(a)** shows a quasi-probability distribution in terms of the so-called Wigner function $W(P, Q)$ which spans the phase space of field quadratures P and Q. Red dashed outline illustrates the $1/e$-contour of the vacuum fluctuations (vacuum state). One can suppress vacuum fluctuations by squeezing them in one direction (and respectively, antisqueezing them in the orthogonal direction, in order to leave the Heisenberg relation for quadrature variances intact $(\Delta P)^2 \cdot (\Delta Q)^2 \geq 1$). Plot **(b)** presents an alternative illustration of the vacuum and squeezed vacuum states in terms of the propagating field amplitude as a function of time. Red dashed lines denote the variance level of vacuum fluctuations. Grey colored outline corresponds to the squeezed state. One can note that, at certain moments of time, the field fluctuations are below the vacuum threshold (vacuum squeezing) or above (antisqueezing). Such propagating squeezed states are highly nonclassical photonic states which can be exploited for various purposes of quantum information processing.

phase ϕ_{LO} [45]. The mixer down-converts the squeezed input signal to zero frequency. The power spectral density P at the mixer output is directly proportional to a certain quadrature variance of the squeezed signal. This specific quadrature is determined by the LO phase ϕ_{LO}. In this way, we can investigate the variance in different quadrature directions by changing ϕ_{LO}. From the theory of a flux-driven JPA presented in Ref. [17], we obtain

$$P = \left| J_{\mathrm{b}} + |K_{\mathrm{b}}| e^{i(2\phi_{\mathrm{LO}} - \pi/2)} \right|^2 + \left| J_{\mathrm{c}} + |K_{\mathrm{c}}| e^{i(2\phi_{\mathrm{LO}} - \pi/2)} \right|^2 , \tag{1.48}$$

where the first term describes the degenerate signal gain with

$$J_{\mathrm{b}} = \frac{\epsilon^2 \omega_0^2 + (\kappa_{\mathrm{ext}}^2 - \kappa_{\mathrm{int}}^2)/4}{\epsilon^2 \omega_0^2 - \kappa^2/4} \qquad \text{and} \qquad K_{\mathrm{b}} = \frac{-i\epsilon\kappa_{\mathrm{ext}}\omega_0}{\epsilon^2 \omega_0^2 - \kappa^2/4} , \tag{1.49}$$

and the second term describes the noise added by the loss channel with

$$J_{\mathrm{c}} = \frac{\kappa/2\sqrt{\kappa_{\mathrm{ext}}\kappa_{\mathrm{int}}}}{\epsilon^2 \omega_0^2 - \kappa^2/4} \qquad \text{and} \qquad K_{\mathrm{c}} = \frac{-i\epsilon\sqrt{\kappa_{\mathrm{ext}}\kappa_{\mathrm{int}}}\omega_0}{\epsilon^2 \omega_0^2 - \kappa^2/4} . \tag{1.50}$$

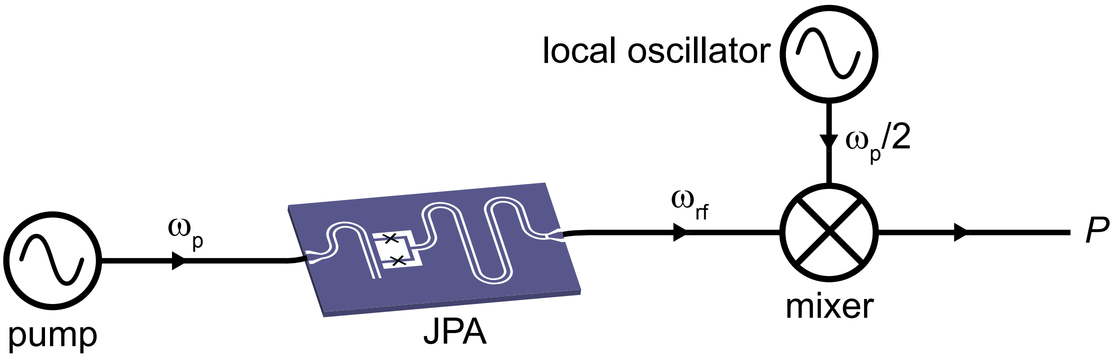

Figure 1.7: Measurement scheme of squeezing properties of a flux-driven JPA which is pumped at a frequency ω_p. The squeezed signal around the frequency $\omega_\mathrm{rf} = \omega_\mathrm{p}/2$ is down-converted to zero frequency by a mixer which is driven by a local oscillator with frequency $\omega_\mathrm{p}/2$ and phase ϕ_LO. The power spectral density P at the mixer output is directly proportional to the variance in different quadrature directions of the squeezed signal.

For a given phase ϕ_LO, P provides the gain for the corresponding quadrature as shown in Fig. 1.5 (a). For $\phi_\mathrm{LO} = \pi/4$, we obtain the minimum gain P_min which corresponds to the squeezed quadrature. For the orthogonal antisqueezed quadrature at $\phi_\mathrm{LO} = 3\pi/4$, we obtain the maximum gain P_max. Since the internal quality factor $Q_\mathrm{int} = 1 \cdot 10^6$ is high, we observe $P_\mathrm{max} \cdot P_\mathrm{min} \simeq 1$. This observation corresponds to noiseless degenerate amplification discussed in the previous subsection, and therefore, the produced squeezed state is pure. In Fig. 1.5 (b), we show how Q_int influences the maximum and minimum quadrature gains. In general, the antisqueezed quadrature is only slightly affected by internal losses while the squeezed quadrature drastically depends on Q_int. We note that, in contrast to the degenerate signal gain in Eq. (1.43), it is important to consider the added noise due to the loss channel if the JPA is treated as a squeezer. Without consideration of the loss channel, we would obtain $P_\mathrm{max} \cdot P_\mathrm{min} < 1$ for low enough Q_int which would lead to a violation of the Heisenberg uncertainty, and thus, to an unphysical state generated by the theory.

We can express the Hamiltonian of a pumped JPA in the interaction picture and rotating-wave approximation in the form

$$\hat{H}_\mathrm{int} = i\hbar\frac{\lambda}{2}\left(\hat{a}^2 e^{-i\varphi} - (\hat{a}^\dagger)^2 e^{i\varphi}\right), \tag{1.51}$$

where φ is the pump phase and $\lambda = \omega_0\epsilon$ is the effective nonlinearity due to the frequency modulation induced by the pump tone. As presented in Ref. [46], a direct connection of the JPA interaction Hamiltonian $\hat{H}_\mathrm{int}$ to the squeezing operator can be made. For $\varphi = 0$, the Heisenberg equation of motion is

$$\frac{d}{dt}\hat{a}(t) = \frac{1}{i\hbar}[\hat{a}(t),\, \hat{H}_\mathrm{int}] = -\lambda\hat{a}^\dagger(t)\,, \tag{1.52}$$

which is solved by $\hat{a}(t) = \hat{a}(0)\cosh(\lambda t) - \hat{a}^\dagger(0)\sinh(\lambda t)$. This solution coincides with the action of the squeeze operator on the annihilation operator. Furthermore, the unitary evolution under the action of the Hamiltonian $\hat{H}_{\text{int}}$ is given by

$$\hat{U}(t) = \exp\left[-\frac{i}{\hbar}\hat{H}_{\text{int}}t\right] = \exp\left[\frac{\lambda}{2}\left(\hat{a}^2 e^{-i\varphi} - (\hat{a}^\dagger)^2 e^{i\varphi}\right)t\right]. \tag{1.53}$$

By introducing the dimensionless interaction time $r = \lambda t$, we recreate the original squeezing operator

$$\hat{U}(t) = \hat{S}(\xi) = \exp\left(\frac{1}{2}\xi^* \hat{a}^2 - \frac{1}{2}\xi(\hat{a}^\dagger)^2\right), \tag{1.54}$$

with $\xi = re^{i\varphi}$.

In practice, JPAs always produce two-mode squeezed (TMS) states due to their naturally finite bandwidth. Here, correlations exist between quadratures of frequency modes which are symmetric around half the pump frequency [47, 32]. During the parametric process in the JPA, photons in these upper and lower sideband modes are generated from a single pump photon. Consequently, it is intuitively clear that these modes should be correlated.

Task 12: Bonus – Squeezing

How much squeezing would you expect to generate with a flux-driven JPA for a given nondegenerate amplification gain G under ideal conditions?

2 Experimental Setup

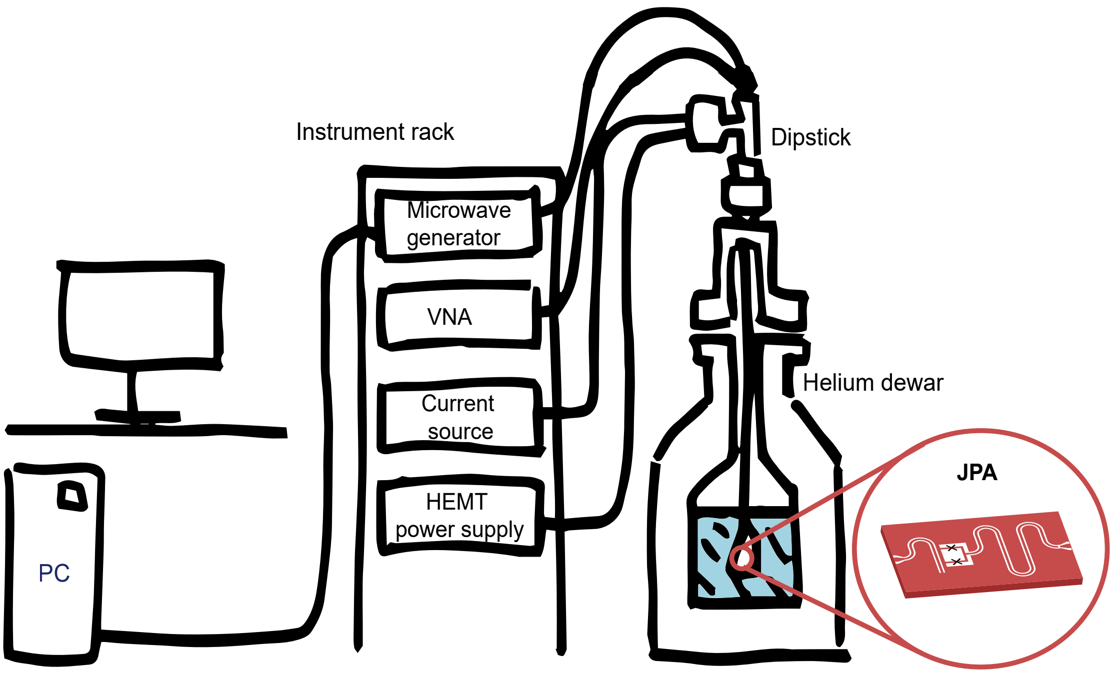

Figure 2.1: Experiment overview.

This chapter focuses on the experimental set-up and relevant procedures required to successfully characterize the flux-driven superconducting JPA and achieve the goals (i)-(iii) highlighted in the abstract. A schematic drawing of the whole set-up is shown in Fig. 2.1. As one can see, it consists of the room temperature control part and the cryogenic counterpart. The former includes a Vector Network Analyzer (VNA) for sending and detecting weak microwave signals, a microwave source for generating strong microwave signals as required for pumping of the JPA, a dc current source for biasing of the magnetic JPA coil, a HEMT power supply for operating a cryogenic microwave preamplifier, and a PC for remote control of all aforementioned devices. The latter, cryogenic counterpart, consists of a dewar with liquid helium and a simple cryogenic measurement apparatus which we will call the "dipstick". This dipstick carries all crucial cryogenic components including the JPA itself.

2.1 JPA sample & microwave packaging

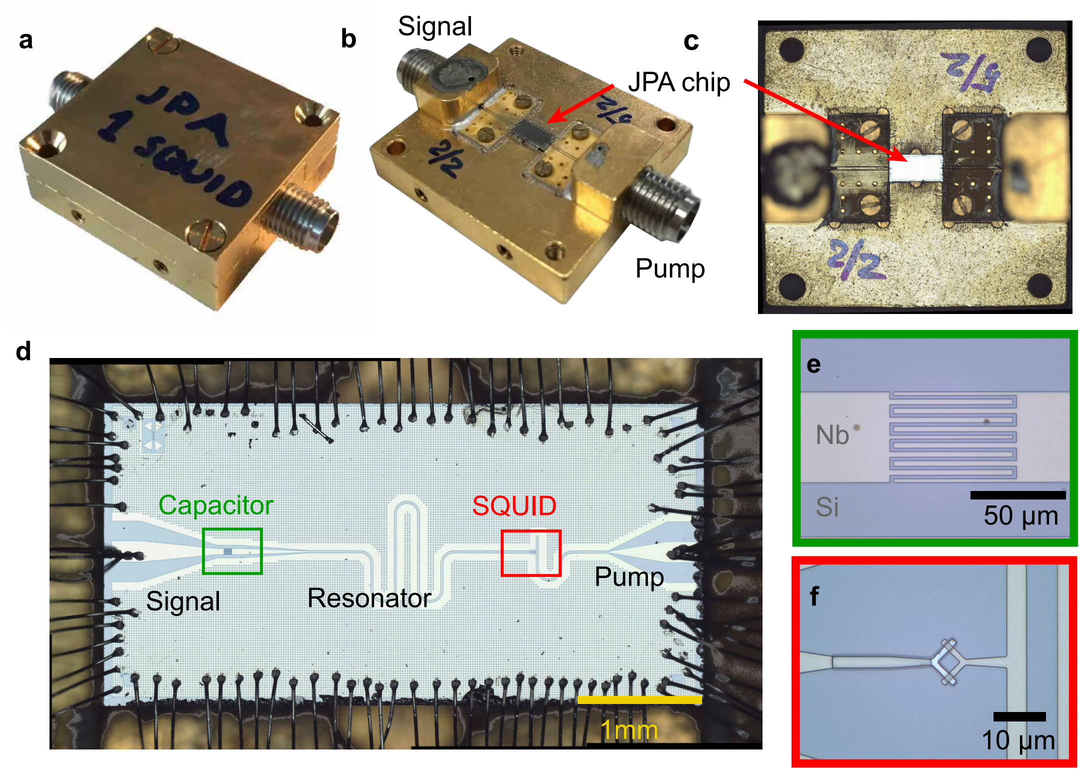

Figure 2.2: Packaged Josephson parametric amplifier. **a** Closed JPA sample holder with SMA-compatible microwave connectors. **b** Opened JPA sample holder. **c** Top view of the inside of the JPA sample holder. The JPA chip is placed in the center of holder connected to two printed circuit boards providing impedance-matched microwave interface for input, output and pump signals. **d** Close-up of the bonded superconducting niobium JPA chip. Green and red rectangles highlight the areas with the coupling capacitor and dc-SQUID, respectively. **e** Close-up of the JPA input capacitor which allows for coupling between incoming external microwave signals and the internal JPA mode. **f** Close-up of the dc-SQUID area. This is the heart of our JPA, which gives rise to the JPA magnetic field tunability. The latter is the result of quantum phase interference in the dc-SQUID and can be exploited for quantum-limited parametric amplification, squeezing, and entanglement generation.

Our JPA is fabricated using a thin-film trilayer niobium process on a silicon substrate. This process allows to form both the coplanar resonator and Josephson junctions (see Figs. 2.2d,e,f for details) in order to implement a tunable superconducting cavity, as discussed earlier in the Theory chapter. Furthermore, one requires to interface the resulting JPA chip with the external microwave waveguides and devices. This task is achieved by using a specific microwave sample holder (shown in Figs. 2.2a,b,c) and aluminum bonding wires (visible as black wires in Fig. 2.2d). These bonds allow for a low inductance connection between the JPA and external microwave waveguides, thus, ensuring proper impedance matching for propagating quantum microwave signals. Later on, all microwave signals are guided through standardized cables with SMA connectors (visible as a part of the sample holder in Figs. 2.2a,b).

Task 13: dc-SQUID

From the size of the SQUID (Fig. 2.2)f, estimate the required magnetic field to create one flux quantum $\Phi_0 = \frac{h}{2e}$ threading through the dc-SQUID.

2.2 Cryogenic signal routing

The cryogenic part of our experiment is illustrated by Fig. 2.3. In order to tune the magnetic flux to the SQUID, we use a superconducting coil mounted directly on top of the JPA sample holder (Fig. 2.3b). Figure 2.3c, shows the signal routing and connections

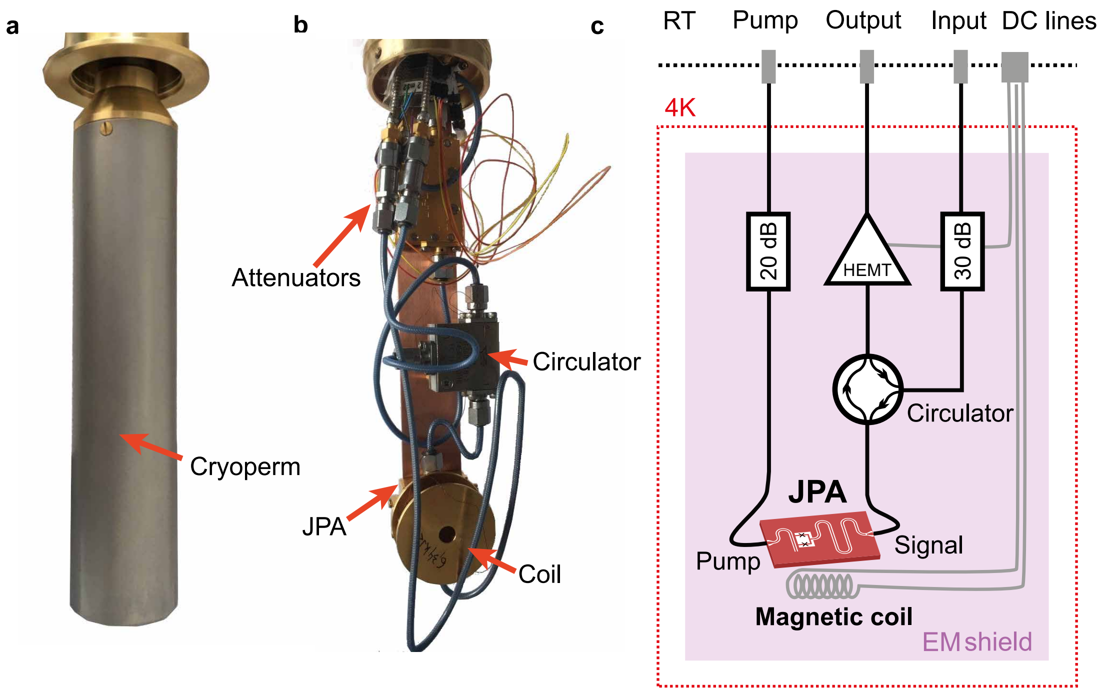

Figure 2.3: Cryogenic part of the dipstick. **a** Cryoperm magnetic shield. **b** Photo of the cryogenic set-up. **c** Experimental cryogenic schematics.

in the cryogenic part of our experiment. We measure the JPA response by sending a weak microwave probe tone to the corresponding input port and detecting a reflected signal. The circulator is used in order to separate these input and output (reflected) signals. The cryogenic HEMT amplifier is used to amplify the output JPA signal in order to increase its signal-to-noise ration and reduce time required for signal averaging. Both the pump and input microwave lines are equipped with microwave attenuators, which act as power dividers. They are needed in order to reduce room temperature thermal noise coming with microwave signals and thermalize it to the cryogenic temperatures of liquid helium $\simeq 4\,\mathrm{K}$. The cryoperm magnetic shield is used to protect the JPA from stray magnetic field (e.g., Earth's magnetic field).

Task 14: Signal flow

Why is it useful to attenuate input and pump signals at temperatures $T = 4\,\mathrm{K}$? What difference would it make to attenuate these signals at room temperatures? Why do we use a circulator in the signal path? Why are there no attenuators in the output line?

2.3 Room temperature filters

Signal filtering is important to remove various unwanted modes from the probe and pump microwave signals going to the JPA. These unwanted contributions may arise due to different sources, such as local WiFi and cell networks, intermodulation effects in microwave generators and VNAs, among others. Therefore, we use an extra set of specific band-pass microwave filters at the top of the dipstick. We expect our JPA resonant frequencies to be in the range of 5-6 GHz and filter out all other spectral components by using a specific filter shown in Fig. 2.5a. The pump line is filtered accordingly under the condition that $\omega_p = 2\omega_s$.

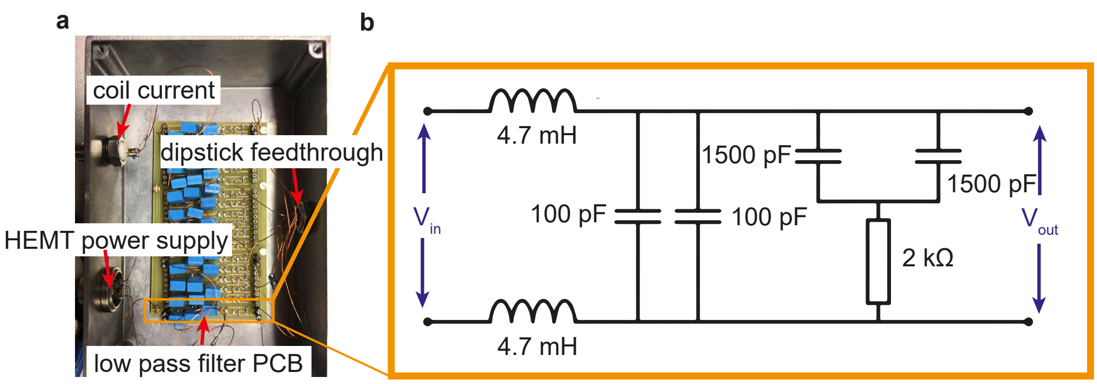

Figure 2.4: Low-pass filter box. **a** Photo of the internal configuration. **b** Equivalent electrical circuit.

Additionally, we use a set of dc lines to power the HEMT amplifier and control bias current through the magnetic coil. These dc lines should be filtered as well with a custom-made low-pass filter with the cutt-off frequency of around 100 kHz (see Fig. 2.4 for details).

Task 15: Microwave filtering

Assume the JPA working resonance frequency of around 6.2 GHz and a set of the following available microwave filters: band-pass 4-5 GHz, low-pass 3 GHz, band-pass 4-8 GHz, high-pass 8 GHz, band-pass 10-13 GHz. Which ones would you use for the signal and pump microwave lines in the current JPA experiment? Why?

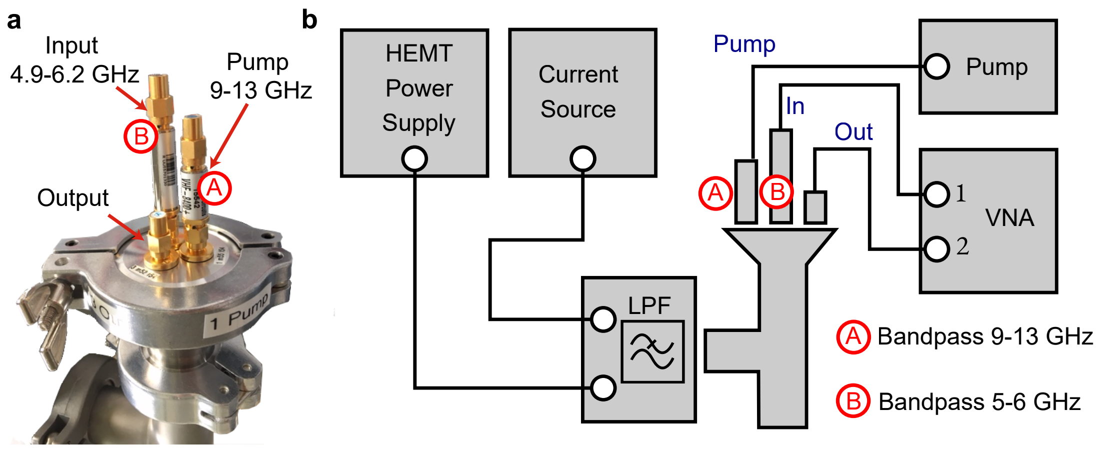

Figure 2.5: Cable connection schematics. **a** Photo of the top flange of the dipstick with three microwave ports. **b** Extended schematics of cable connections between room temperature devices and the dipstick ports. Markers A and B mark the microwave pump and signal input connections and filters, respectively.

2.4 Electronic measurement equipment

Assuming that all the signal and power lines are connected correctly within the cryogenic dipstick, we have to consider room temperature connections to measurement electronics. Here, our central measurement tools are a microwave generator, a Vector Network Analyzer (VNA), and a dc current source. Specifically, we use R&S ZND-K1 VNA for sending and detecting microwave probe signals, as required for measuring the JPA resonant response. Microwave generator R&S SGS100A is used for generation of strong microwave signals as required for parametric pumping and amplification with our flux-driven JPA. The dc source current is represented by Keithley 2401 which allows for flexible and precise control of the dc bias currents running through the magnetic coil on top of the JPA. In addition to these devices, we have to use a specific power supply to power the HEMT amplifier. Figure 2.6 illustrates all these devices and respective interfaces. In Fig. 2.5, you can see that port 1 of the VNA is connected to the input line at

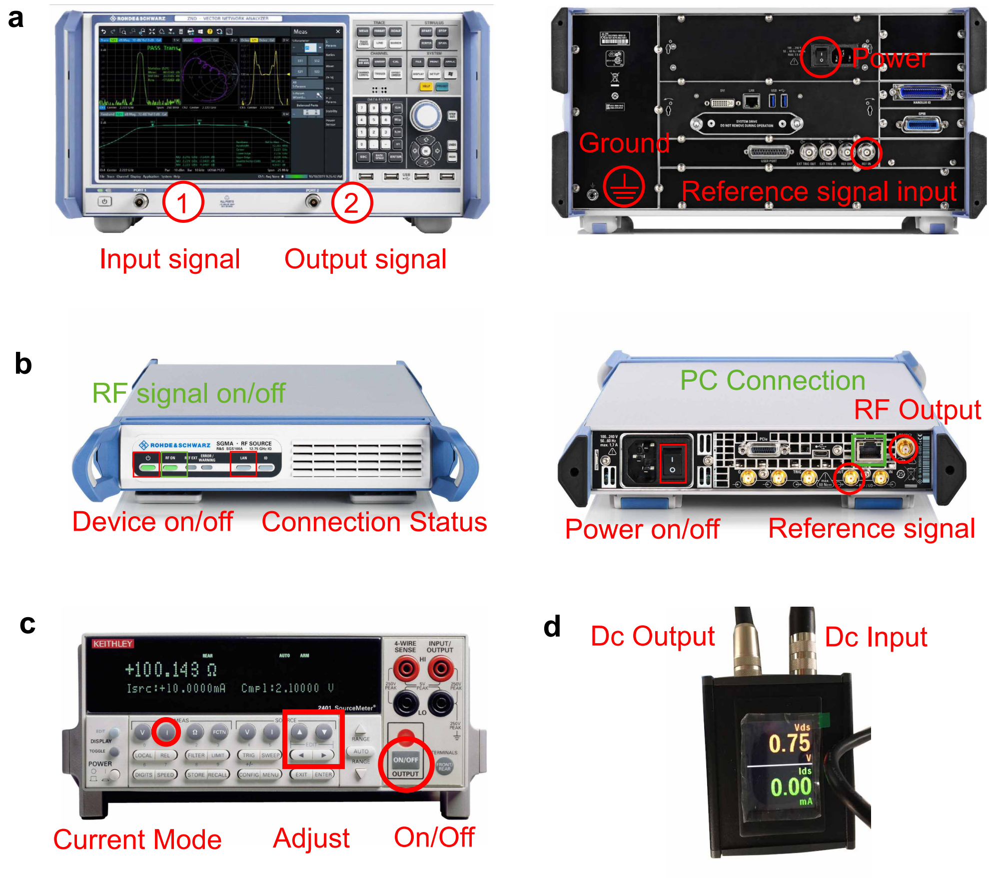

Figure 2.6: Photos and important elements of room temperature instruments. **a** Front and rear views of R&S ZND-K1 vector network analyzer, **b** Front and rear views of R&S SGS100A microwave generator, **c** Front view of Keithley 2401 current source. **d** Power supply of the cryogenic HEMT amplifier.

the dipstick. As Port 1 is the only port that can generate a signal, we are always measure the corresponding transmission from Port 1 to Port 2 via the respective S-characteristic $S21$.

Safety remarks

- **VNA & microwave generator**: always wear a grounding hand band when working with the Vector Network Analyzer (VNA) and microwave generator in order to protect these devices from electrostatic discharge.
- **Current source**: don't exceed 1 mA of dc current flowing through the supercon-

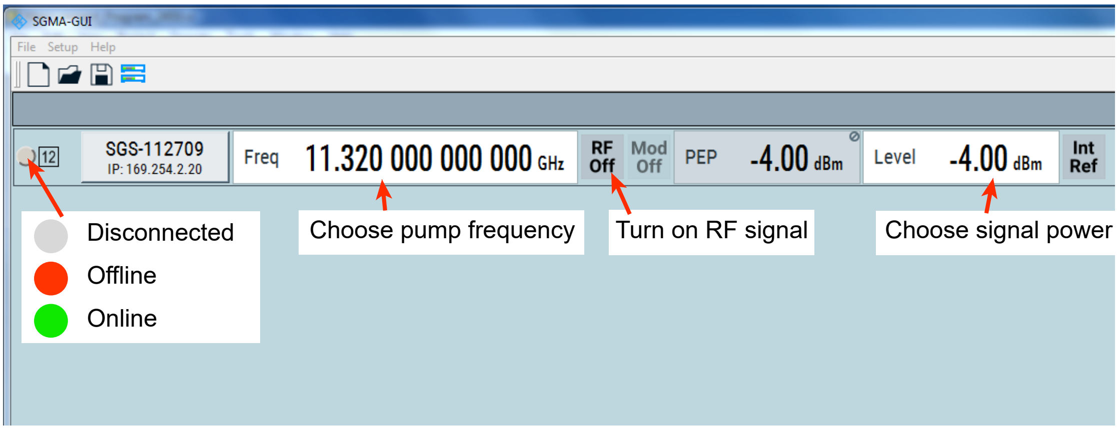

Figure 2.7: Graphical user interface (available only via a remote PC) of R&S SGS100A microwave generator.

ducting coil in order to avoid excessive magnetic fields affecting the sample, which may lead to degradation of the JPA performance.

Task 16: Signal Power

Assuming the JPA resonance frequency $f = 6\,\mathrm{GHz}$, its bandwidth $BW = 50\,\mathrm{MHz}$, and the VNA output power $P = 0\,\mathrm{dBm}$, estimate the total attenuation (in dB units) of the input line required to create 1 photon in the JPA resonator.

3 Measurement

3.1 Safety introduction

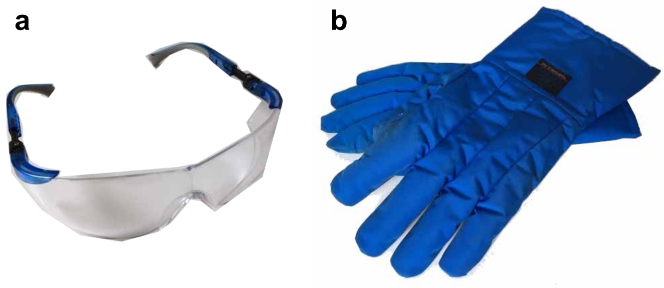

Figure 3.1: Safety equipment. **a** Cryogenic safety gloves. **b** Safety goggles.

The experiment involves sensitive electronic equipment and cryogenic fluids. In order to ensure personal safety and long lifetime of the equipment, students have to follow the following guidelines:

- Don't touch any open conductors.
- When working with any microwave cables, **always wear the electrostatic band connected to the VNA ground**.
- When fastening SMA connectors, always use torque specialized wrenches.
- Always use safety goggles and the cryogenic safety gloves when handling helium or touching potentially cold parts.
- During the cooldown procedure, the dipstick must be lowered into the dewar very slowly. Never open the rubber flange and the pinch lock at the same time.
- Don't move, shake, or tip the dewar.
- Leave the door open during the experiment.
- The helium dewar must always be connected to the return helium network to avoid potentially dangerous overpressure.
- Liquid helium has a 757-fold volume increase when evaporating. The dewar may contain up to 100 l of liquid helium, whereas the volume of an elevator cabin is 8000 l. Therefore, it is strictly forbidden to enter the elevator cabin together with the transported dewar with liquid helium.

Task 17: Liquid helium

Calculate how much liquid helium one would need to evaporate to fill the entire elevator volume with He gas. Compare the result with the the dewar volume.

3.2 Checking the Helium Level

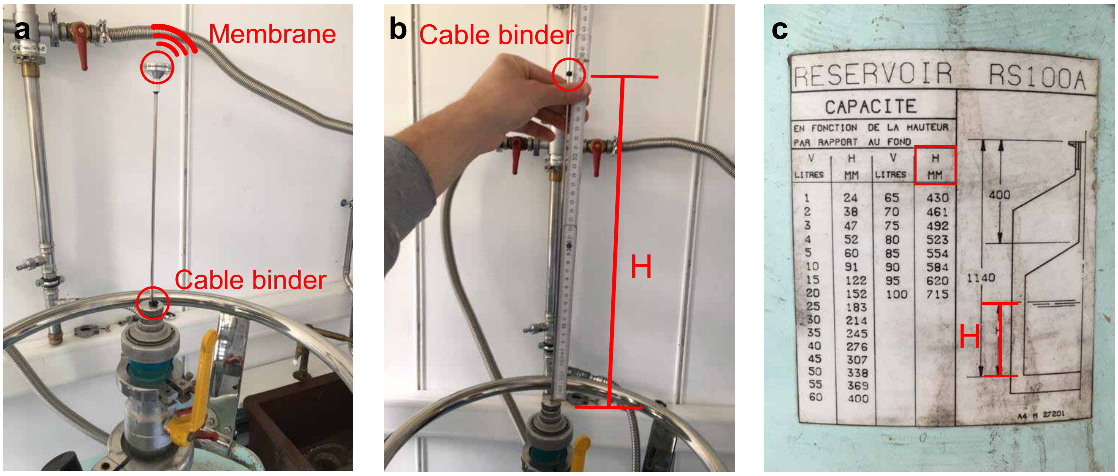

Figure 3.2: Helium level measurements. **a** Insert the helium level meter tool and adjust the cable binder. **b** Find an acoustic discontinuity by lowering the level meter into the dewar and measure the distance H. **c** Estimate the volume of liquid helium in the dewar by using the calibration table on the dewar side. Important! The dewar must contain at least 50 liters of liquid helium prior the cooldown.

Get the following equipment from the WMI helium hall: a helium level meter, a whiteboard marker, a cloth, a folding ruler.

1. Mount the dipstick onto the dewar, open the cone closing and slowly lower the helium level meter until you touch the ground of the dewar.
2. Now, adjust the cable binder at the top of the level meter to the level of the dewar as shown in Figure 3.2a.
3. Slowly lift the level meter until you hear an acoustic change in the membrane resonance frequency. Use the folding ruler to measure the level of liquid helium in the dewar and use the table at the dewar side in order to estimate the corresponding liquid helium volume.
4. Finally, use a whiteboard marker and write down the date and volume of liquid helium in the respective field on the dewar itself.

3.3 Mounting the dipstick onto the dewar

1. Ensure that the cryoperm shield is fully inside of the protective brass cylinder before mounting of the dipstick to the dewar.
2. Ensure that everyone operating the dipstick and dewar are wearing safety goggles and cryogenic gloves during the cooldown.
3. The supervisor should bring the dipstick to the dewar.
4. The student loosens the wing screw of the clamp at the dewar lid.
5. The student removes the lid, the supervisor places the dipstick on top of the dewar. Afterwards, the student fixates the dipstick using the previously loosened clamp.

3.4 Cooling down the sample rod

There are two ways to hold the dipstick in place: by using either the rubber flange, or the pinch lock (see Fig. 3.4). You should open the pinch lock for adjusting the dipstick vertical position, while keeping the rubber flange closed at a reasonably close distance ($\leq$ 15 cm). You should keep one of the two closed at all times to prevent the dipstick from crashing into the dewar in order to avoid very dangerous overpressure spikes.

3.5 Cryogenic measurements

1. Turn ON the room temperature control electronics. Then, make sure all outputs are OFF.
2. Connect the dc lines and microwave cables according to Fig.2.5. Additionally, connect the VNA Port 1 to the dipstick input via an external attenuator chain fixed at the rack (-40 dB). Strictly follow the safety guidelines.
3. Press the VNA preset button. Set the VNA output power to -20 dBm. Set the VNA frequency range to 5-6.5 GHz. Identify the JPA resonance dip (usually around 6 GHz) in the absence of external magnetic field and without the microwave pump.
4. Make sure that the dc current source output is set to zero. Switch the current source range to 1 mA. Switch ON the current source output (actual current must be still zero). Slowly sweep the current in 1 μA steps in the range between -200 μA and 200 μA. Observe and record smooth tuning of the JPA resonance dip as a function of the current. Identify the corresponding JPA bias current period and flux/current conversion ratio.
5. Identify a suitable amplification working point (usually, it is around $\Phi_0/4$ in terms of magnetic flux through the dc-SQUID) for the JPA. Record the JPA frequency f_{JPA} and a corresponding S21 curve. Adjust the microwave generator frequency

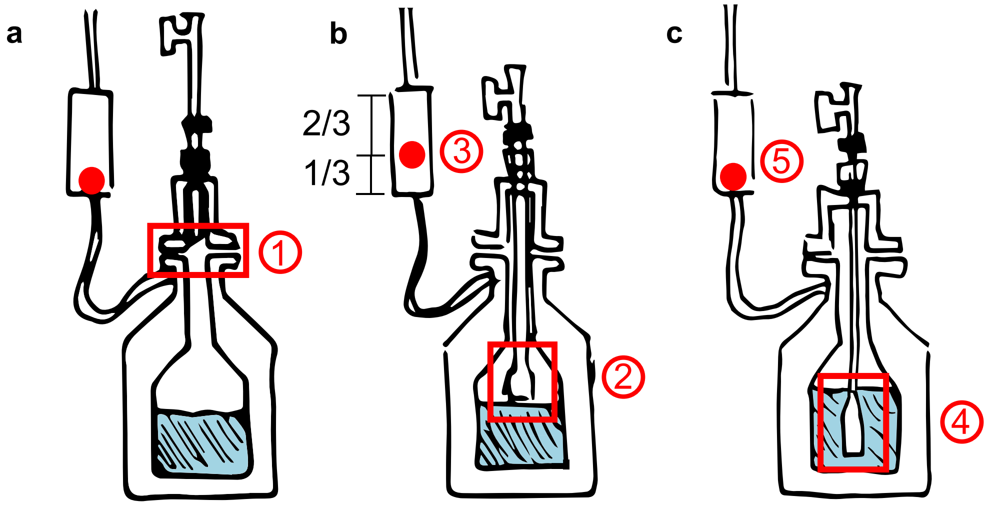

Figure 3.3: Cooldown procedure. **a** Mount the dipstick at the dewar top (1). **b** In order to pre-cool the cryogenic set-up, slowly, over approximately 30 minutes, lower down the dipstick down into the dewar, however, without touching the surface of liquid helium yet (2). An approximate criterion for the pre-cooling speed is given by the vertical position of the table tennis ball (marked with red circle here) in the helium return line. The ball should never rise above 33 % of the overall tube height as indicated by (3) in order to ensure somewhat adiabatic cooling, preserve liquid helium, and protect the cryogenic set-up from excessive thermal stress. **c** After the pre-cooling is complete, lower the dipstick slowly into the bottom position but slightly over the dewar bottm (4). Do not hit the dewar bottom! When the dipstick is safely at its lowest position and the overpressure in the helium return line is negligible (5) - the dipstick is ready for cryogenic measurements.

to $f_{\mathrm{pump}} = 2f_{\mathrm{JPA}}$ and power to 0 dBm. Turn ON the microwave generator. Adjust the pump power and frequency a little bit to achieve a maximum JPA gain G. Record and save all experimental data.

6. If $G < 10\,\mathrm{dB}$, try to find adjust the JPA working point by changing the bias current until you find the parameter regime with $G > 10\,\mathrm{dB}$. Make sure you have all data needed for the report. Check chapter 4 for details.

7. In the end of the experiment, switch OFF all outputs (VNA, microwave generator, current source). Disconnect all cables from the dipstick. Switch OFF all room temperature electronics. Proceed with a warm-up procedure as described below.

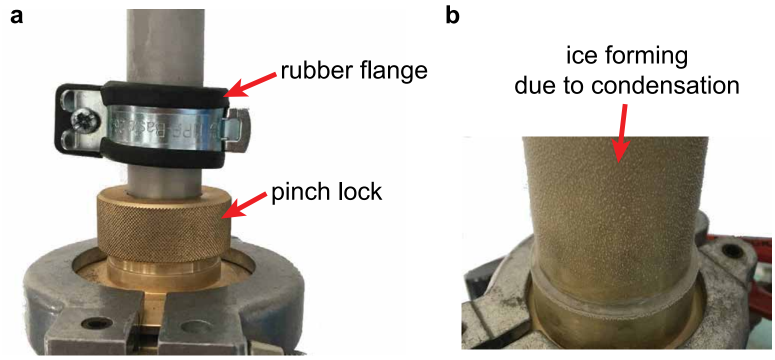

Figure 3.4: Important parts of the cryogenic dipstick. **a** The rubber flange is the second line of security and must always be fastened, especially when the pinch lock is opened. **b** Water condenses after warmup on the brass cylinder. Here, you can observe ice formation on the outside of the protective brass cylinder during the warm-up.

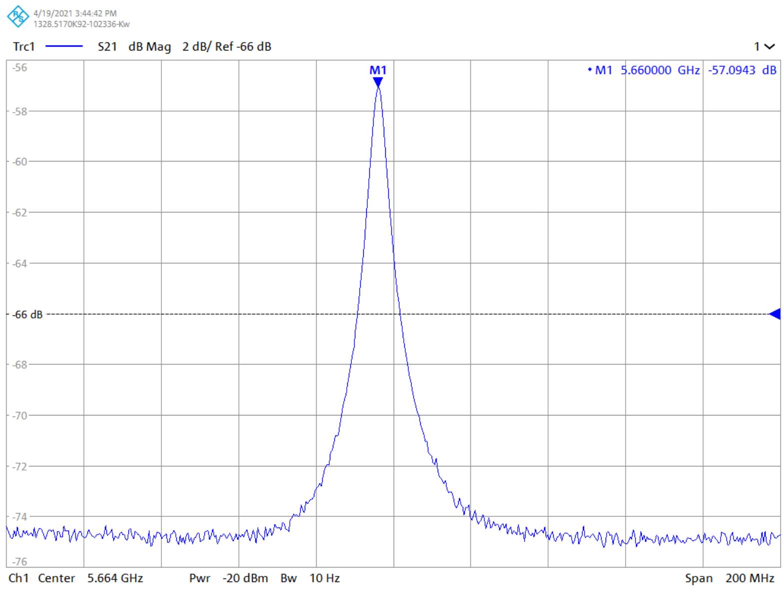

Figure 3.5: Exemplary S21 transmission measurements with VNA of the JPA sample in the presence of the pump tone at frequency $f_p \simeq 11.33\,\mathrm{GHz}$. Here, marker "M1" corresponds to the maximum of the JPA amplification response.

3.6 Warm-up procedure

A warming-up procedure is the final step of the student lab. Here, it is important to follow strict guidelines in order to avoid damages to the cryogenic set-up:

1. Disconnect all the dc and microwave wires and the filter box from the dipstick.

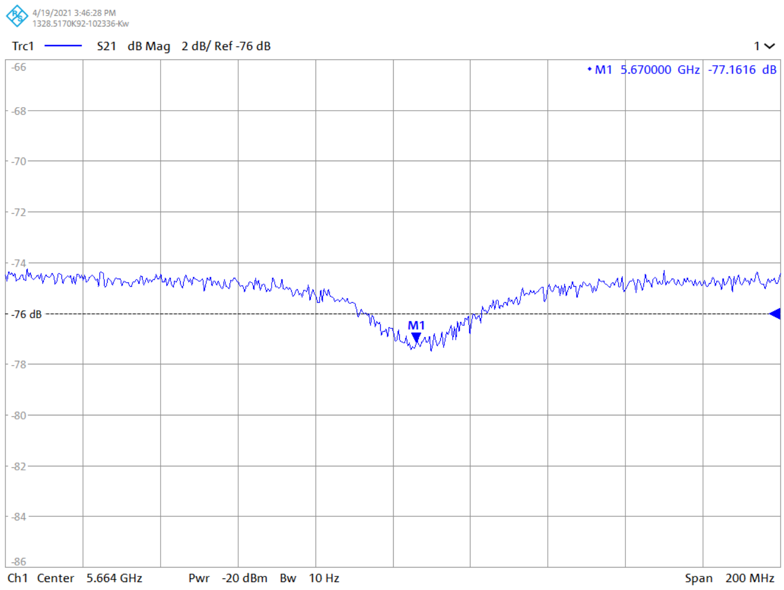

Figure 3.6: Exemplary S21 transmission measurements with VNA of the JPA sample in the absence of the pump tone. Marker "M1" corresponds to the JPA resonance frequency.

2. Pull up the dipstick to approximately half of its height out of the dewar (so, that the cryoperm shield inside of the dewar must be positioned safely above the liquid helium surface) and leave it in this position for around **10-15 minutes**.

3. Slowly pull up the dipstick to its upper position, so that the cryoperm shield is fully located inside of the brass cylinder. Leave the dipstick tightly fixed (use both the rubber flange and pinch lock) in this upper position for **3-4 hours**. In order to optimize everyone's time, it is usually reasonable to leave the final step of the dipstick extraction to the supervisor. **It is crucial for the stable and long-living operation of the whole experiment that the dipstick is extracted from the dewar only when the it (dipstick) is fully thermalized at room temperatures.** Premature extraction of the dipstick, while it is still at temperatures below 0 °C, will lead to water condensing over various elements of the cryogenic set-up and may lead to a quick degradation and damages to the HEMT amplifier and superconducting JPA sample.

4 Writing the report

4.1 Preparation

Please read through the manual and answer the tasks in a written format before attending the experiment. These tasks should help you to critically consider the most important points regarding theory, experiment, and safety of the current practicum.

4.2 Evaluation

Your report should be as concise as possible. Briefly motivate the topic and highlight the most important equations. Describe your experimental procedure. For the description of the setup and equipment you can rely on the manual. Discuss your results and compare it to a data set of another student groups, or to the one shown in the current manual.

Your report should provide the plots as shown in Fig. 4.1, demonstrating the flux dependency and amplification gain $G > 10\,\mathrm{dB}$. Try to explain your observations in the framework of the provided theory of flxu-driven JPAs.

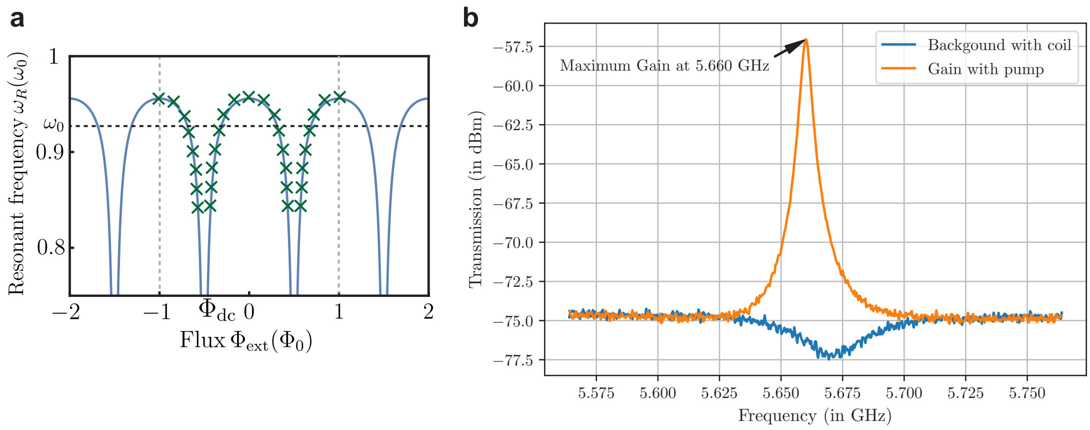

Figure 4.1: Exemplary expected plots of students' report. **a** JPA flux curve. Here, green crosses illustrate experimentally measured data points, while blue curve depicts theoretically expected behaviour according to Eq. 1.37. **b** Experimental JPA frequency-dependent S21 characteristics for the cases with the pump tone off and on.

Bibliography

[1] B.D. D Josephson. “Possible new effects in superconductive tunnelling”. In: *Phys. Lett.* 1.7 (July 1962), pp. 251–253.

[2] P. E. Schmidt. “Widerstand zwecklos: Die makroskopische Wellenfunktion als Grundlage der Theorie von Supraleitung und Suprafluidität”. In: *Junge Wissenschaft* 84 (2009), pp. 38–43.

[3] W. Buckel and R. Kleiner. *Superconductivity.* Wiley, Weinheim, 2004.

[4] Rudolf Gross and Achim Marx. *Festkörperphysik.* Oldenbourg Verlag, München, 2012.

[5] John Clarke and Alex I Braginski. *The SQUID Handbook: Fundamentals and Technology of SQUIDs and SQUID Systems.* Wiley, Weinheim, 2004.

[6] G. Wendin and V. S. Shumeiko. “Superconducting Quantum Circuits, Qubits and Computing”. In: *Handbook of Theoretical and Computational Nanotechnology.* Ed. by M. Rieth and W. Schommers. American Scientific Publishers, Los Angeles, 2006, pp. 223–309.

[7] S M Girvin, M H Devoret, and R J Schoelkopf. “Circuit QED and engineering charge-based superconducting qubits”. In: *Phys. Scr.* T137.T137 (2009), p. 014012.

[8] G. Wendin. “Quantum information processing with superconducting circuits: a review”. In: *Rep. Prog. Phys.* 80.10 (Oct. 2017), p. 106001.

[9] M. Tinkham. *Introduction to Superconductivity.* McGraw-Hill Inc., New York, 1996.

[10] M. Sandberg et al. “Tuning the field in a microwave resonator faster than the photon lifetime”. In: *Appl. Phys. Lett.* 92.20 (May 2008), p. 203501.

[11] Valérie Lefevre-Seguin et al. “Thermal activation of a hysteretic dc superconducting quantum interference device from its different zero-voltage states”. In: *Phys. Rev. B* 46.9 (Dec. 1992), p. 5507.

[12] Matteo Mariantoni et al. “Implementing the Quantum von Neumann Architecture with Superconducting Circuits”. In: *Science* 334.6052 (2011), pp. 61–65.

[13] Edwar Xie et al. “Compact 3D quantum memory”. In: *Appl. Phys. Lett.* 112.20 (2018), p. 202601.

[14] T. Niemczyk et al. “Circuit quantum electrodynamics in the ultrastrong-coupling regime”. In: *Nat. Phys.* 6.10 (2010), pp. 772–776.

[15] D. M. Pozar. *Microwave Engineering.* Wiley, Hoboken, 2012.

[16] M. Göppl et al. “Coplanar waveguide resonators for circuit quantum electrodynamics”. In: *J. Appl. Phys.* 104.11 (2008), p. 113904.

[17] T Yamamoto, K Koshino, and Y Nakamura. “Parametric Amplifier and Oscillator Based on Josephson Junction Circuitry”. In: *Principles and Methods of Quantum Information Technologies.* Ed. by Yoshihisa Yamamoto and Kouichi Semba. Springer Japan, Tokyo, 2016, pp. 495–513.

[18] David S. Wisbey et al. “Effect of metal/substrate interfaces on radio-frequency loss in superconducting coplanar waveguides”. In: *J. Appl. Phys.* 108.9 (Nov. 2010), p. 093918.

[19] Christopher L Holloway and Edward F. Kuester. “Edge shape effects and quasi-closed form expressions for the conductor loss of microstrip lines”. In: *Radio Sci.* 29.3 (May 1994), pp. 539–559.

[20] T. Yamamoto et al. “Flux-driven Josephson parametric amplifier”. In: *Appl. Phys. Lett.* 93.4 (July 2008), p. 042510.

[21] M. Wallquist, V. S. Shumeiko, and G. Wendin. “Selective coupling of superconducting charge qubits mediated by a tunable stripline cavity”. In: *Phys. Rev. B* 74.22 (Dec. 2006), p. 224506.

[22] Waltraut Wustmann and Vitaly Shumeiko. “Parametric resonance in tunable superconducting cavities”. In: *Phys. Rev. B* 87.18 (May 2013), p. 184501.

[23] J. Bourassa et al. “Josephson-junction-embedded transmission-line resonators: From Kerr medium to in-line transmon”. In: *Phys. Rev. A* 86.1 (July 2012), p. 013814.

[24] P Bhupathi et al. “Transient Dynamics of a Superconducting Nonlinear Oscillator”. In: *Phys. Rev. Appl.* 5.2 (Dec. 2016), p. 024002.

[25] W. H. Louisell, A. Yariv, and A. E. Siegman. “Quantum Fluctuations and Noise in Parametric Processes. I.” In: *Phys. Rev.* 124.6 (Dec. 1961), p. 1646.

[26] J P Gordon, W H Louisell, and L R Walker. “Quantum Fluctuations and Noise in Parametric Processes. II”. In: *Phys. Rev.* 129.1 (Jan. 1963), p. 481.

[27] B Yurke et al. “Observation of 4.2-K equilibrium-noise squeezing via a Josephson-parametric amplifier”. In: *Phys. Rev. Lett.* 60.9 (Feb. 1988), p. 764.

[28] B Yurke et al. “Observation of parametric amplification and deamplification in a Josephson parametric amplifier”. In: *Phys. Rev. A* 39.5 (Mar. 1989), p. 2519.

[29] M. A. Castellanos-Beltran and K. W. Lehnert. “Widely tunable parametric amplifier based on a superconducting quantum interference device array resonator”. In: *Appl. Phys. Lett.* 91.8 (Aug. 2007), p. 083509.

[30] N. Bergeal et al. “Phase-preserving amplification near the quantum limit with a Josephson ring modulator”. In: *Nature* 465.7294 (May 2010), pp. 64–68.

[31] M. Hatridge et al. “Dispersive magnetometry with a quantum limited SQUID parametric amplifier”. In: *Phys. Rev. B* 83.13 (Apr. 2011), p. 134501.

[32] C. Eichler et al. "Quantum-Limited Amplification and Entanglement in Coupled Nonlinear Resonators". In: *Phys. Rev. Lett.* 113.11 (Sept. 2014), p. 110502.

[33] Chris Macklin et al. "A near-quantum-limited Josephson traveling-wave parametric amplifier". In: *Science* 350.6258 (Oct. 2015), pp. 307–310.

[34] A. A. Clerk et al. "Introduction to quantum noise, measurement, and amplification". In: *Rev. Mod. Phys.* 82.2 (Apr. 2010), p. 1155.

[35] P. CARRUTHERS and MICHAEL MARTIN NIETO. "Phase and Angle Variables in Quantum Mechanics". In: *Rev. Mod. Phys.* 40 (2 Apr. 1968), pp. 411–440.

[36] Z R Lin et al. "Single-shot readout of a superconducting flux qubit with a flux-driven Josephson parametric amplifier". In: *Appl. Phys. Lett.* 103.13 (Sept. 2013), p. 132602.

[37] A. Eddins et al. "High-Efficiency Measurement of an Artificial Atom Embedded in a Parametric Amplifier". In: *Phys. Rev. X* 9.1 (Jan. 2019), p. 011004.

[38] Wolfgang Pfaff et al. "Controlled release of multiphoton quantum states from a microwave cavity memory". In: *Nat. Phys.* 13.9 (Sept. 2017), pp. 882–887.

[39] L Steffen et al. "Deterministic quantum teleportation with feed-forward in a solid state system". In: *Nature* 500.7462 (Aug. 2013), pp. 319–322.

[40] H. A. Haus and J. A. Mullen. "Quantum Noise in Linear Amplifiers". In: *Phys. Rev.* 128.5 (Dec. 1962), p. 2407.

[41] Carlton M. Caves. "Quantum limits on noise in linear amplifiers". In: *Phys. Rev. D* 26.8 (Oct. 1982), p. 1817.

[42] L. Zhong et al. "Squeezing with a flux-driven Josephson parametric amplifier". In: *New J. Phys.* 15.12 (Dec. 2013), p. 125013.

[43] R. Movshovich et al. "Observation of zero-point noise squeezing via a Josephson-parametric amplifier". In: *Phys. Rev. Lett.* 65.12 (Sept. 1990), p. 1419.

[44] D. F. Walls and G. J. Milburn. *Quantum Optics*. Springer, Berlin Heidelberg, 2008.

[45] Bernard Yurke and Eyal Buks. "Performance of cavity-parametric amplifiers, employing Kerr nonlinearites, in the presence of two-photon loss". In: *J. Light. Technol.* 24.12 (Dec. 2006), pp. 5054–5066.

[46] Samuel L. Braunstein and Peter van Loock. "Quantum information with continuous variables". In: *Rev. Mod. Phys.* 77.2 (June 2005), p. 513.

[47] C. Eichler et al. "Observation of Two-Mode Squeezing in the Microwave Frequency Domain". In: *Phys. Rev. Lett.* 107.11 (Sept. 2011), p. 113601.